(4)

NUMERICAL MODELLING OF SHOCKS IN GASES AND METALS

MRL-RR-8-89

AR-005-742

M.B. TYNDALL

MATERIALS RESEARCH LABORATORY

DSTO

Numerical Modelling of Shocks in Gases and Metals

M.B. Tyndall

MRL Research Report
MRL-RR-8-89

1989

Abstract

Results are presented for a range of one-dimensional shock wave problems in gaseous and metallic materials. These problems were solved numerically using Flux-Corrected Transport (FCT). FCT is a numerical technique which achieves high resolution without non-physical oscillations, especially in regions of steep gradients such as shock fronts.

These types of problem involve solving the Eulerian inviscid fluid flow equations, namely the continuity equation, conservation of momentum and conservation of energy, with an appropriate equation of state. For gaseous materials the ideal gas equation of state was used and for metallic materials the "stiffened-gas" or the Mie-Grüneisen equation of state. Shock wave problems in gases included the one-dimensional shock tube problem, a shock wave hitting a density discontinuity and shocks of equal magnitude colliding. Using the "stiffened-gas" equation of state and the Mie-Grüneisen equation of state similar types of problems were solved for metallic materials, for example, a shock propagating through a piece of metal.

A discussion of the performance of FCT to accurately model these problems is given. Currently work is being done on adding elastic-plastic (or viscous) terms and heat conduction terms to the fluid flow equations, to improve the description of flow in a solid material.

Published by DSTO Materials Research Laboratory
Cordite Avenue, Maribyrnong, Victoria 3032, Australia
Telephone: (03) 319 3887
Fax: (03) 318 4536

AR No. 005-742

Approved for Public Release

Author

Moya Tyndall completed a B.Sc.(Hons) degree at Monash University in 1986, majoring in Applied Mathematics. She began working as an experimental officer in the Explosives Division at Materials Research Laboratory in July 1987. In March 1988, after being made a DSTO Research Fellow, Moya started a Ph.D. degree in the Department of Mathematics at Monash University. For her Ph.D. thesis, Moya is developing a two-dimensional numerical model that will study the propagation of shock waves through solid materials.

Contents

Numerical Modelling of Shocks in Gases and Metals

1. Introduction

What happens when two solids collide? For impacts which do not involve large deformations a description of the behaviour in terms of elastic, plastic and shock wave propagation is needed. The main aim of this work is to develop a numerical model which can describe the impacts of solids (involving no large deformations) in one and two dimensions. Before elastic-plastic properties of impacting solids can be considered a thorough understanding of shocks in solids is required.

We start by modelling shocks in an inviscid gas. Using Flux-Corrected Transport (FCT), the Eulerian inviscid fluid flow equations, governing the conservation of mass, momentum and energy together with the ideal gas equation are solved for a range of one-dimensional shock wave problems in gases. FCT resolves shock fronts over two to three grid points and moving discontinuities over six grid points, without any undershoots or overshoots. By choosing a different equation of state, which can describe the properties of a solid material, similar types of problems are solved in a solid. The ideal gas equation is replaced with either the "stiffened-gas" equation of state or the Mie-Grüneisen equation of state. Treating a solid as an inviscid fluid is found to be unsatisfactory and the inclusion of viscous and heat conduction terms is needed. These terms give an improved description of shock wave behaviour in a solid material.

This report gives the details of the one-dimensional problems attempted so far in gases and solids. The system of equations and equations of state are given in section 2, details of the types of FCT used to solve these equations are in section 3, a description of the problems attempted is in section 4, a discussion of the results in section 5 and some concluding remarks are in section 6.

2. Equations

In this section the equations of motion for a compressible fluid (in one dimension) are given, along with some simple equations of state for gases and metals.

2.1 The system of equations

In one dimension the Eulerian inviscid fluid flow equations can be written in conservation (or vector) form as

$$\frac{\partial \mathbf{U}}{\partial t} + \frac{\partial \mathbf{F}(\mathbf{U})}{\partial x} = 0 \tag{2.1}$$

where

$$\mathbf{U} = \begin{pmatrix} \rho \\ \rho u \\ E \end{pmatrix}, \qquad \mathbf{F}(\mathbf{U}) = \begin{pmatrix} \rho u \\ \rho u^2 + p \\ (E + p)u \end{pmatrix},$$

ρ is the density, u the particle velocity, E the total energy per unit volume and p the pressure. Heat conduction effects have been ignored (they will be discussed later). The total energy per unit volume can be expressed as the sum of the heat and kinetic energies,

$$E = \rho I + \tfrac{1}{2}\rho u^2 \tag{2.2}$$

where I is the internal energy per unit mass. To complete this system of equations an appropriate equation of state needs to be defined. Usually, the equation of state defines the pressure as a function of density and internal energy,

$$p = p(\rho, I). \tag{2.3}$$

2.2 Equations of state

In the literature there is a wide range of equations of state based on both theoretical and experimental results. These equations can be extremely complicated and can describe a varied range of material behaviour. For the types of problems solved here the ideal gas equation and simple metal equations of state will be sufficient.

For an ideal gas, equation (2.3) is defined as

$$p = (\gamma - 1)\rho I \tag{2.4}$$

where γ is the ratio of specific heats.

An equation of state that can adequately describe both gases and metals is the Mie-Grüneisen equation of state (Harlow & Amsden 1971),

$$p = p_H + \gamma_s \rho (I - I_H) \tag{2.5}$$

where

$$p_H = \frac{\rho_o c_o^2 (1 - \frac{\rho_o}{\rho})}{[1 - s(1 - \frac{\rho_o}{\rho})]^2} \tag{2.6}$$

$$I_H = \frac{1}{2}\left(\frac{c_o(1 - \frac{\rho_o}{\rho})}{1 - s(1 - \frac{\rho_o}{\rho})} \right)^2 \tag{2.7}$$

$$\gamma_s = 2s - 1 \tag{2.8}$$

p_H is the pressure along the Hugoniot at density ρ, I_H the corresponding internal energy per unit mass, ρ_o the normal density of the material, c_o the speed of sound in the unshocked material, γ_s the Grüneisen ratio and s the shock velocity versus particle velocity slope. The shock velocity U is related to the particle velocity by the empirical Hugoniot relationship

$$U = c_o + su. \tag{2.9}$$

If the Hugoniot cannot be represented by a straight line when plotting shock velocity versus particle velocity, then an alternative form of equation (2.9) has to be used.

The expressions for p_H and I_H (equations (2.6) and (2.7)) can be derived from the Rankine-Hugoniot conditions across a shock-front (Hayes 1973)

$$\frac{\rho_o}{\rho} = 1 - \frac{u - u_o}{U - u_o} \tag{2.10}$$

$$p - p_o = \rho_o(U - u_o)(u - u_o) \tag{2.11}$$

$$I - I_o = \tfrac{1}{2}(p + p_o)(\tfrac{1}{\rho_o} - \tfrac{1}{\rho}) \tag{2.12}$$

where the shock velocity is given by equation (2.9). The subscript '$_o$', in the above equations refers to the unshocked material.

If the density varies only slightly from the normal density, then the Mie-Grüneisen equation can be simplified to the form

$$p = c_o^2(\rho - \rho_o) + (\gamma - 1)\rho I, \tag{2.13}$$

which is called the "stiffened-gas" equation of state (Harlow & Amsden 1971), where $\gamma - 1 \equiv \gamma_s$. For large internal energies this equation behaves similarly to the ideal gas equation (equation (2.4)).

3. Numerical Scheme

A finite difference approximation to equation (2.1) is in conservation (or 'flux') form when it can be written in the form,

$$\mathbf{U}_i^{n+1} = \mathbf{U}_i^n - \frac{\Delta t}{\Delta x}\left[\mathbf{T}_{i+\frac{1}{2}} - \mathbf{T}_{i-\frac{1}{2}}\right]. \tag{3.1}$$

Here $\mathbf{U}_i^n$ is the value of $\mathbf{U}$ at the ith grid point for the nth time step. An evenly spaced grid is assumed. The $\mathbf{T}_{i\pm\frac{1}{2}}$ are called transportive fluxes, and are functions of $\mathbf{U}$ and $\mathbf{F}$ at the nth time step.

When trying to model shock waves numerically we encounter many difficulties. Some are due to the steep gradients involved (a shock in an inviscid fluid is a point discontinuity) and others due to the numerical method being used, for example, excessive implicit diffusion and non-physical oscillations. When choosing a suitable numerical method to model shock waves, we seek a method which will give a monotonic solution (no non-physical oscillations) and can accurately model any discontinuities, for example, spreading shock fronts (in a gas) over no more than four grid points. Flux-corrected transport (FCT) is a technique developed in a series of papers by Boris & Book (1973), Book, Boris & Hain (1975) and Boris & Book (1976) which gives a monotonic solution with a high level of accuracy. To illustrate the principles of FCT consider the advection of a square wave (Fig. 1). For a constant velocity field $u(x,t) = u$, equation (2.1) reduces to

$$\frac{\partial \rho}{\partial t} + u\frac{\partial \rho}{\partial x} = 0 \tag{3.2}$$

where only the density profile of the square wave is considered.

If a low-order scheme, such as the donor cell method (Roache 1972), is used to model a square wave, the solution (Fig. 1a) suffers from excessive diffusion. Alternatively, if a high-order scheme, such as the Lax-Wendroff method (Sod 1978), is used, the solution (Fig. 1b) suffers from non-physical oscillations. When FCT is used (Figs. 1c and 1d, whose differences of which will be discussed later) a highly accurate, monotonic solution is obtained. FCT constructs a transportive flux which is a weighted average of a flux computed by a low-order *monotonic* scheme and a flux computed by a high-order scheme. The weighting procedure blends the low and high order schemes in such a way that the high-order scheme is used to as great as extent as possible, subject to the constraint that no under or overshoots are introduced into the solution.

The Zalesak (1979) FCT procedure (hereinafter ZFCT) is as follows:

(1) Compute $\mathbf{T}_{i+\frac{1}{2}}^{L(n)}$, the transportive flux given by some low-order monotonic scheme.

(2) Compute $\mathbf{T}_{i+\frac{1}{2}}^{H(n)}$, the transportive flux given by some high order (second or above) scheme.

(3) D· the 'anti-diffusive' fluxes:

$$\mathbf{A}_{i+\frac{1}{2}}^{(n)} = \mathbf{T}_{i+\frac{1}{2}}^{H(n)} - \mathbf{T}_{i+\frac{1}{2}}^{L(n)}$$

(4) Compute the updated low-order ('transported and diffused') solution:

$$\mathbf{U}_i^{td} = \mathbf{U}_i^n - \frac{\Delta t}{\Delta x}\left[\mathbf{T}_{i+\frac{1}{2}}^{L(n)} - \mathbf{T}_{i-\frac{1}{2}}^{L(n)}\right]$$

(5) Limit the anti-diffusive fluxes $\mathbf{A}_{i+\frac{1}{2}}$ in a way such that *no existing extrema are accentuated and no new extrema are created* in the solution that are not in $\mathbf{U}^{td}$ or $\mathbf{U}^n$.

$$\mathbf{A}_{i+\frac{1}{2}}^{C(n)} = \mathbf{C}_{i+\frac{1}{2}}\mathbf{A}_{i+\frac{1}{2}}^{(n)} \qquad 0 \leq \mathbf{C}_{i+\frac{1}{2}} \leq 1$$

(6) Apply the limited antidiffusive fluxes:

$$\mathbf{U}_i^{n+1} = \mathbf{U}_i^{td} - \frac{\Delta t}{\Delta x}\left[\mathbf{A}_{i+\frac{1}{2}}^{C(n)} - \mathbf{A}_{i-\frac{1}{2}}^{C(n)}\right]$$

The critical step in the above is step 5, which is referred to as "flux-correction" or "flux-limiting". If the $\mathbf{C}_{i+\frac{1}{2}}$ coefficients in step 5 are zero then the low-order, monotonic solution is obtained, but if they are equal to one (in regions where non-physical oscillations are absent) then the high-order solution is obtained. In regions where non-physical oscillations are present the $\mathbf{C}_{i+\frac{1}{2}}$ coefficients are calculated in such a way that at each point enough implicit nonlinear diffusion is added to damp out these oscillations. The "flux-limiting" process ensures that $\mathbf{U}_i^{n+1}$ lies within the range $\mathbf{U}_{min}$ to $\mathbf{U}_{max}$ where $\mathbf{U}_{min}$ and $\mathbf{U}_{max}$ are determined from examination of local $\mathbf{U}^n$ and $\mathbf{U}^{td}$ values. Details of this 'flux-limiting' process (in particular how the $\mathbf{C}_{i+\frac{1}{2}}$ coefficients are calculated) will not be discussed here and can be found in Zalesak (1979) FCT can be classed as an implicit artificial viscosity or implicit damping method since implicit diffusion or viscosity is added without appearing explicitly in the equations (Roache 1972).

Zalesak (1979) has placed the theory of Boris and Book's original FCT (hereinafter BBFCT) in a simple, generalised format which can accomodate more liberal flux-limiting techniques, including his multi-dimensional flux-limiter. Compared to BBFCT, ZFCT has an improved flux-limiting stage, but does not have the low phase errors of BBFCT.

By modifying ZFCT Dietachmayer (1987) constructed a scheme that has the low phase errors of BBFCT with the gererality of ZFCT. This scheme, called "re-ordered

ZFCT"(hereinafter RZFCT), is based on ZFCT, but is used in such a way that time levels are not mixed in the anti-diffusive step (see step 6 above).

The procedure is as follows (Dietachmayer 1987):

(1) Compute $\mathbf{T}^{L(n)}_{i+\frac{1}{2}}$, the transportive flux given by some low-order monotonic scheme.

(2) Obtain the updated low-order ('transported and diffused') solution $\mathbf{U}^{*}_{i}$, using the low-order monotonic scheme.

$$\mathbf{U}^{*}_{i} = \mathbf{U}^{n}_{i} - \frac{\Delta t}{\Delta x}\left[\mathbf{T}^{L(n)}_{i+\frac{1}{2}} - \mathbf{T}^{L(n)}_{i-\frac{1}{2}}\right]$$

(3) Compute the low-order fluxes at $(*)$ level

$$\mathbf{T}^{L(*)}_{i+\frac{1}{2}}.$$

(4) Compute the high-order fluxes at $(*)$ level

$$\mathbf{\Gamma}^{H(*)}_{i+\frac{1}{2}}.$$

(5) Calculate the 'anti-diffusive' fluxes:

$$\mathbf{A}^{*}_{i+\frac{1}{2}} = \mathbf{T}^{H(*)}_{i+\frac{1}{2}} - \mathbf{T}^{L(*)}_{i+\frac{1}{2}}$$

(6) Limit the anti-diffusive fluxes

$$\mathbf{A}^{C(*)}_{i+\frac{1}{2}} = \mathbf{C}_{i+\frac{1}{2}}\mathbf{A}^{*}_{i+\frac{1}{2}} \qquad 0 \leq \mathbf{C}_{i+\frac{1}{2}} \leq 1$$

(7) Implement the antidiffusive step,

$$\mathbf{U}^{n+1}_{i} = \mathbf{U}^{*}_{i} - \frac{\Delta t}{\Delta x}\left[\mathbf{A}^{C(*)}_{i+\frac{1}{2}} - \mathbf{A}^{C(*)}_{i-\frac{1}{2}}\right].$$

No extra phase errors are introduced in RZFCT, making this procedure more accurate than ZFCT. Dietachmayer (1987) tested a wide range of schemes, including ZFCT and BBFCT, and found RZFCT to be the most accurate of all the schemes.

Returning to the square wave problem discussed earlier, we can compare the ZFCT and RZFCT solutions (Figs. 1c and 1d, respectively). The only noticeable difference between these solutions is the smaller amount of rounding in the leading edge of the square wave when RZFCT is used and the low phase errors of RZFCT is the main reason for this difference. These results do not show the significant phase lag of ZFCT that is found in the results of Dietachmayer (1987). This difference is due to the higher resolution used in this study. The ZFCT and RZFCT solutions clip the top left-hand corner and bottom right-hand corner, and to a lesser extent the top right-hand corner of the square wave. These inaccuracies are due to the limitations of the high-order scheme (Fig. 1b), and can be eliminated by choosing a more accurate scheme than the Lax-Wendroff method.

4. Some One-Dimensional Test Problems

Some simple one-dimensional problems were chosen to test ZFCT and RZFCT (see section 3) for their accuracy and suitability to model shock waves.

4.1 Gases

Four problems were used to test the ability of ZFCT and RZFCT to model shock waves in a gaseous material with the ideal gas equation (equation (2.4)). Rusanov's method was used to calculate the low-order fluxes and the Lax-Wendroff method was used to calculate the high-order fluxes. Details of these numerical methods can be found in Roache (1972) or Sod (1978).

The Shock Tube

The first problem was the one-dimensional shock tube problem, which is a stringent test for the non-linear systems described by equation (2.1) (see Sod 1978). It is a simple problem in which a diaphragm separates two regions of different pressures and densities in a semi-infinite tube. The fluid on each side of the diaphragm is an ideal gas which is at rest at time $t = 0$. To the left of the diaphragm, the gas is initially at a higher density and pressure than on the right.

Once the diaphragm is ruptured ($t > 0$), a rarefaction propagates into the high-pressure gas and a shock wave followed by a contact discontinuity, propagates into the low-pressure gas. Details of the exact solution can be found in Harlow & Amsden (1971) and Tyndall (1988).

One hundred points were taken each side of the diaphragm (which was positioned at $x = 0$) with $\Delta x = 0.025$. The ratio of specific heats, γ, was 1.4 in equation (2.4). The initial conditions were

$$\rho = 1.0 \qquad p = 1.0 \qquad u = 0.0 \qquad x < 0$$

and

$$\rho = 0.125 \qquad p = 0.1 \qquad u = 0.0 \qquad x > 0.$$

The Steady Shock

The second problem was the propagation of a one-dimensional shock through a uniform polytropic gas, at rest, ahead of the shock. All variables downstream of the shock were known and an initial density discontinuity was assumed. All the other variables, including the shock velocity U, were derived from the Rankine-Hugoniot conditions (see appendix for details). A schematic diagram of this problem is given in Fig. 2 and the initial conditions are in Table 1.

Shock hitting a density discontinuity

For the third problem, the steady shock described above was propagated into a stationary density discontinuity. This problem is illustrated in Fig. 3 and the initial conditions are given in Table 1.

The collision of two shocks

This problem consisted of two shocks of equal magnitude colliding (see Fig. 4). Initial conditions for this problem are given in Table 1.

4.2 Metals

The steady shock problem and the collision of two shocks were the problems used to test the ability of ZFCT and RZFCT to model shock waves in a metallic material. These problems involved only small density changes, so the "stiffened-gas" equation of state was used. Recall, that the Mie-Grüneisen equation can be simplified to the "stiffened-gas" equation of state when the density varies slightly from the normal density (see section 3.2). Roe's upwind scheme (see Roe 1981) was used to calculate the low-order fluxes and the Lax-Wendroff method was used to calculate the high-order fluxes. Three types of material were used in these simulations, aluminium, copper and stainless steel. The physical data needed for the Mie-Grüneisen and "stiffened-gas" equations of state for each of these materials is given in Table 2. Since they all behaved similarly, only the details and results for aluminium are given here.

The Steady Shock

This problem is equivalent to the steady shock problem in a gas. A one-dimensional weak shock was propagated through aluminium (see Fig. 2). All variables downstream of the shock were specified and an initial density discontinuity was assumed (1% compression). All variables upstream of the shock and the shock velocity U were derived from the Rankine-Hugoniot conditions in the same way as the steady shock problem in a gas (see appendix). The initial conditions for this problem are set out in Table 3.

The collision of two shocks

Two types of collisions were modelled in aluminium, one where two shocks of equal magnitude collided and the other where two shocks of different magnitudes collided. The initial conditions for these problems are also set out in Table 3.

5. Results and Discussion

In this section the results are presented for the problems described in the previous section.

5.1 Gases

The Shock Tube

The solution to the shock tube problem using ZFCT is shown in Fig. 5. It follows the general form of the exact solution. The contact discontinuity has been slightly diffused and the shock front has been well resolved (only two to three points wide). This solution agrees well with the solution given by Sod (1978), using BBFCT (Boris and Book's FCT). Neither of these solutions is monotonic. In the density profile there is an undershoot at the end of the rarefaction ($x = 0$) and a slight overshoot in the contact discontinuity ($x = 1.0$). This behaviour is also present in the pressure, velocity and energy profiles. This non-monotonic behaviour is not caused by phase errors or the flux-correction stage (see section 3) but by the initial conditions. If we integrate numerically starting from the exact solution at some time $t > 0$, rather then rupturing the diaphragm at $t = 0$, these undershoots and overshoots do not appear. In Fig. 6, the exact solution at $t = 0.5$ was used as the initial conditions, then ZFCT was used to calculate a solution at $t = 1.0$ (one hundred time steps later). There are no undershoots at the end of the rarefaction and no overshoots in the contact discontinuity, and the shock front and

contact discontinuity are the same widths as Fig. 5. The small irregularities at $x = 0.9$ in the pressure and velocity profiles are due to inaccuracies in the numerical scheme in the region of the contact discontinuity, across which the theoretical pressures and velocities are continuous.

The shock tube problem was also solved using RZFCT, see Fig. 7. Comparing Figs. 5 and 7, RZFCT gives a more accurate solution than ZFCT. The contact discontinuity is less rounded, the shock front is only two points wide and there is only a slight undershoot at the end of the rarefaction. Using the one-dimensional advection equation, Dietachmayer (1987) tested a range of monotonic advection schemes and found that the best results were obtained using RZFCT. Hence the remainder of the problems studied here were solved using RZFCT.

The Steady Shock

The propagation of a shock through a gas is shown in Fig. 8. The shock front is represented by three points and does not diffuse as it travels through the gas. The shock front moved through the gas with shock velocity $U = 1.19$. Apart from the small wiggles in the solution near $x = 0$, the solution is correct to three significant figures, but in the region of the wiggles the solution is only correct to two significant figures. These wiggles in the solution are artifacts of the initial conditions, which will be discussed later.

Shock hitting a density discontinuity

In Figs. 9 and 10 a series of plots show the interaction of a shock hitting a density discontinuity. Shortly before time $t = 1.0$ (Figs. 9b and 10b), the shock (with shock velocity $U = 1.67$) collided with the density discontinuity. If we look at the density and energy at $t = 1.0$ (Figs. 9b and 10b), a shock has begun to form that will travel through the more dense stationary gas and another weaker shock has been reflected from the discontinuity. The pressure and particle velocity in between the two shocks should be constant but, since the shock that travels through the more dense gas is still forming, there is a small dip in the pressure and the particle velocity is slightly variable in this region. At later times $t = 1.5$ and $t = 2.5$ (Figs. 9c, 9d, 10c and 10d) the shocks can be clearly seen and the pressure and particle velocity are constant in this region. The shock travelling through the more dense gas is two to three grid points wide and the reflected shock is three to four grid points wide. Both shocks do not diffuse as they travel through the gas. The shock travelling through the more dense gas and the reflected shock propagate with shock velocities $U = 0.97$ and $U = -0.58$, respectively. The solution is correct to three significant figures except for the shock velocities after the collision, which are correct to two significant figures.

The collision of two shocks

The problem of two colliding shocks is shown in Fig. 11. Before the shocks collide they

are travelling with shock velocities $U = 1.67$ and $U = -1.67$. After the collision at $x = 0$ the shocks are reflected and travel with shock velocities $U = 1.01$ and $U = -1.01$. At $t = 1.0$ there is a dip region in the density, centered at $x = 0$ and a slight overshoot and undershoot in the particle velocity in the same region. These, like the wiggles in the steady shock problem above, are caused by the initial conditions, where the collision of the two shocks can be considered as the initial stage for the reflected shocks. At a later time $t = 2.0$ (Fig. 11b) the dip region in density transforms into a region of wiggles and the velocity is monotonic. Apart from these irregularities, the shocks are well resolved and do not diffuse as they travel through the gas. The solution is correct to three significant figures except for the irregularities described above, where the solution is correct to two significant figures.

5.2 Metals

The Steady Shock

A one-dimensional weak shock travelling through aluminium,is shown in Fig. 12. The density ratio is small (1% compression) but the pressure, particle velocity and energy ratios are much larger than those of the equivalent gas problem (see Fig. 8).Taking this into consideration, the shock front is resolved extremely well, even though it is wider (about eight points wide) than the shock front in Fig. 8. The shock propagates through the aluminium with shock velocity $U = 5450$ ms^{-1}, which is within 0.4% of the exact shock velocity. The density, particle velocity and pressure are monotonic and involve less that 0.1% error. However, the energy is not monot ic, with a small spike at $x = 0$ m. When there is a larger density discontinuity it is possible to see a corresponding dip in the density at $x = 0$ m. In the region of the spike there is a 13.0% error in the energy and elsewhere there is less than 0.5% error. In this problem the spike does not affect the pressure as the energy term in the equation of state (equation (2.13)) is much smaller than the other terms. This non-monotonic behaviour is caused by the initial conditions, like the wiggles and other irregularities of the gas problems.

We use the steady shock problem to show how the initial conditions cause the irregularities. A general, linearised solution of the fluid flow equations (equation (2.1)) for the density is

$$\rho(x,t) = f(x-(u+c)t) + g(x-(u-c)t) + h(x-ut) \qquad (5.1)$$

where the functions f, g and h are determined by the initial conditions. Initially the shock was located at $x = 0$ m and assumed to be an exact shock, that is, a point discontinuity in an inviscid fluid (Fig. 13). We want to excite a shock wave which will travel with wave speed '$u + c$', that is, the functions g and h are zero and f is non-zero in equation (5.1). When we model the theoretical shock numerically there is a slight smoothing of the discontinuity (Fig. 13) causing the functions g and h to be small

rather than zero. Therefore, we have small amplitude waves travelling with speeds 'u' and '$u - c$' as well as the shock propagating with speed '$u + c$'. The spike in the energy at $x = 0$ m, and the wiggles and other irregularities in the gas problems are these small amplitude waves travelling with speed 'u'. Current work involves including viscous and heat conduction terms in the fluid flow equations, which should give a more accurate discription of the initial stage and diffuse these small contributions. Instead of assuming a shock is a point discontinuity, we should define it as a thin region where viscosity and heat conduction are important.

The collision of two shocks

The collision of two equal strength shocks in aluminium , with shock velocities $U = 5450$ ms^{-1} and $U = -5450$ ms^{-1}, is shown in Figs. 14, 15 and 16. After the collision the shocks are reflected, similar to the collision of two equal strength shocks in a gas (Fig. 11). The reflected shocks travel with shock velocities $U = 5430$ ms^{-1} and $U = -5430$ ms^{-1} which are within 0.4% of the exact shock velocities. Spikes in the energy occur at the initial shock positions ($x = -1.5$ m and $x = 1.5$ m) and at the point of collision ($x = 0$ m). The point of collision is where the shocks change direction, travelling back the way they came, and can be thought of as a new starting position, hence causing a spike to appear and also slight overshoots at the shock fronts. In the region of the spike at $x = 0$ m there is a 6.5% error in the energy and in the region of the overshoots a 1.2% error.

The collision of two shocks of different strengths in aluminium is shown in Figs. 17 and 18. Before the collision the shocks travel with shock velocities $U = 5410$ ms^{-1} and $U = -5450$ ms^{-1} which are within 0.2% and 0.4% of the exact shock velocities, respectively. After the collision the shocks are reflected and travel with shock velocities $U = 5400$ ms^{-1} and $U = -5430$ ms^{-1}, which are within 0.1% of the exact shock velocities. In the region of the spikes at the initial shock positions, $x = -1.5$ m and $x = 2.0$ m, there is a 6.5% and 13.0% error in the energy, respectively. At the point of collision $x = 0.25$ m there is a 2.0% error in the energy.

6. Conclusions

Using Flux-Corrected Transport (FCT), the Eulerian inviscid fluid flow equations were solved for a range of one-dimensional shock wave problems in gases and metals. Heat conduction effects were ignored. FCT was chosen to solve these problems because it gives a *monotonic* solution with a high level of accuracy, especially in regions of steep gradients, such as shock fronts. FCT resolved the shock fronts in gases over no more than four grid points and contact discontinuities over six grid points. In metals, however,

FCT spread shock fronts over eight grid points, but, since the pressure, particle velocity and energy ratios were much larger than an equivalent gas problem, this was to be expected. In gases and to a greater extent in metals the numerical solution exhibited some non-monotonic behaviour, found to be due to effects from the initial conditions and not FCT. In all problems the initial condition was a point discontinuity, that is, a theoretical shock. When the point discontinuity was modelled numerically there was a slight smoothing of the discontinuity causing small amplitude waves to be propagated through the solution. The regions of non-monotonic behaviour in the solutions were these small amplitude waves. To eliminate these small amplitude waves the initial condition should be a thin region where viscosity and heat conduction are important. Apart from the regions of non-monotonic behaviour, the numerical solutions for the problems in gases and solids were within 1.0% of their exact solutions.

Current work includes adding viscous and heat conduction terms in the conservation of momentum and energy equations (equations (2.1)), so that shock waves in solids can be modelled more accurately. Strong shocks will also be modelled using the Mie-Grüneisen equation of state and incorporating elastic-plastic terms in the fluid flow equations.

7. Acknowledgements

I would like to thank Dr Michael Page of Monash University and Dr Don Richardson of MRL for their invaluable discussions and help in preparing this report.

8. References

Boris J.P. and Book D.L., (1973). *Journal of Computational Physics.* **11**, 38.

Boris J.P. and Book D.L., (1976). *Journal of Computational Physics.* **20**, 397.

Book D.L.,Boris J.P. and Hain K., (1975). *Journal of Computational Physics.* **18**, 248.

Dietachmayer G.S., (1987). *On the numerical simulation of small scale intense atmospheric vortices,* PhD thesis, Monash University.

Harlow F.H. and Amsden A.A.,(1971). *Fluid Dynamics,* Report LA-4700, Los Alamos Scientific Laboratory (Reprinted 1980).

Hayes D.B., (1973). Lecture notes from the course *Introduction to stress wave phenomena,* taught during the spring of 1973 at Sandia Laboratories, Albuquerque.

Matuska, D.A. and Osborne, J.J., (1985). HULL Documentation Volume 2, *Hull Users Manual.* Orlando Technology Inc., Florida.

Roache, P.J., (1972). *Computational Fluid Dynamics,* Hermosa Publishers, Albuquerque.

Roe, P.L., (1981). *Journal of Computational Physics.* **43**, 357.

Sod G.A., (1978). *Journal of Computational Physics.* **27**, 1.

Tyndall M.B., (1988). *An analysis of an implicit factored scheme for simulating shock waves,* Report MRL-R-1117, Materials Research Laboratory, Maribyrnong, Victoria.

Zalesak S.T., (1979). *Journal of Computational Physics.* **31**, 335.

9. Appendix

In this appendix, the propagation of a one-dimensional shock through a uniform polytropic gas (see Fig. 2) is considered. Using the Rankine-Hugoniot conditions (equations (2.10)-(2.12)), we can derive the variables upstream of the shock and the shock velocity. To do this, the variables downstream of the shock must be known and also one of the upstream variables, either density, pressure or particle velocity.

We assume an initial density discontinuity of the form

$$\rho_1 = K\rho_2, \tag{A1}$$

where K is an arbitrary constant and the subscript '2' refers to the unshocked region. The material ahead of the shock is at rest,

$$u_2 = 0. \tag{A2}$$

the Rankine-Hugoniot conditions become

$$\frac{1}{K} = 1 - \frac{u_1}{U} \tag{A3}$$

$$p_1 - p_2 = \rho_2 U u_1 \tag{A4}$$

$$I_1 - I_2 = \tfrac{1}{2\rho_2}(p_1 + p_2)(1 - \frac{1}{K}). \tag{A5}$$

Rearranging equation $(A3)$ gives the particle velocity,

$$u_1 = U(1 - \frac{1}{K}). \tag{A6}$$

From the ideal gas equation (equation (2.4)) the internal energy per unit mass can be written in terms of pressure and density,

$$I = \frac{p}{(\gamma - 1)\rho}. \tag{A7}$$

Substituting equation $(A7)$ into $(A5)$ gives an expression for the pressure p_1 in terms of p_2, K and γ,

$$\frac{p_1}{p_2} = \frac{K(\gamma + 1) - (\gamma - 1)}{(\gamma + 1) - K(\gamma - 1)}. \tag{A8}$$

Substituting equations $(A6)$ and $(A8)$ into $(A4)$ gives

$$U^2 = \frac{2\gamma p_2 K}{\rho_2[(\gamma + 1) - K(\gamma - 1)]}. \tag{A9}$$

The pressure of a very strong shock rises to infinity if

$$\frac{\rho_1}{\rho_2} = \frac{\gamma+1}{\gamma-1}, \tag{A10}$$

hence for the shock velocity U to be defined, that is, $U^2 > 0$,

$$\frac{\rho_1}{\rho_2} < \frac{\gamma+1}{\gamma-1}. \tag{A11}$$

All the variables upstream of the shock are now in terms of the initial density ratio K, the pressure in the unshocked region p_2 and the ratio of specific heats γ.

Similar expessions to equations (A6), (A7), (A8) and (A9) can be derived for the Mie-Grüneisen equation of state (see equations (2.5)-(2.8)) and the "stiffened-gas" equation of state (equation (2.13)) when an initial density discontinuity is asssumed (equation (A1)) and the variables in the unshocked region (region 2) are specified.

Table 1

The initial conditions for the shock wave problems in gases, except the shock-tube problem (section 4.1). The two regions in the steady shock problem (Fig. 2) were 1a and 2; the three regions in the shock hitting a density discontinuity (Fig. 3) were 1b, 2 and 3; and, the three regions in the collision of two shocks (Fig. 4) were 1b, 2 and 3b. The ideal gas equation (equation (2.4)) was used, where the ratio of specific heats γ was 1.4.

Region i	Density ρ_i	Pressure p_i	Particle Velocity u_i
1a	0.50	0.275	0.59
1b	0.25	0.275	0.84
2	0.125	0.1	0.0
3a	0.5	0.1	0.0
3b	0.25	0.275	−0.84

Table 2

Physical data needed for the Mie-Grüneisen and the "stiffened-gas" equations of state (from Matuska & Osborne 1985).

Material	Density $\rho_0(\mathrm{kg\,m^{-3}})$	Grüneisen Ratio γ_s	Sound Speed $c_0(\mathrm{m\,s^{-1}})$
Aluminium	2710	1.67	5380
Stainless Steel	7860	2.46	4610
Copper	8900	1.99	3958

Table 3

The initial conditions for the shock wave problems in aluminium (section 4.2). The two regions in the steady shock problem (Fig. 2) were 1a and 2; the three regions in the collision of two equal strength shocks (Fig. 4) were 1a, 2 and 3; and, the three regions in the collision of two unequal strength shocks (Fig. 4) were 1b, 2 and 3.

Region i	Density $\rho_i(\mathrm{kg\,m^{-3}})$	Pressure $p_i(\mathrm{Pa})$	Particle Velocity $u_i(\mathrm{m\,s^{-1}})$
1a	2737	79×10^7	54
1b	2724	39×10^7	27
2	2710	0	0
3	2737	79×10^7	-54

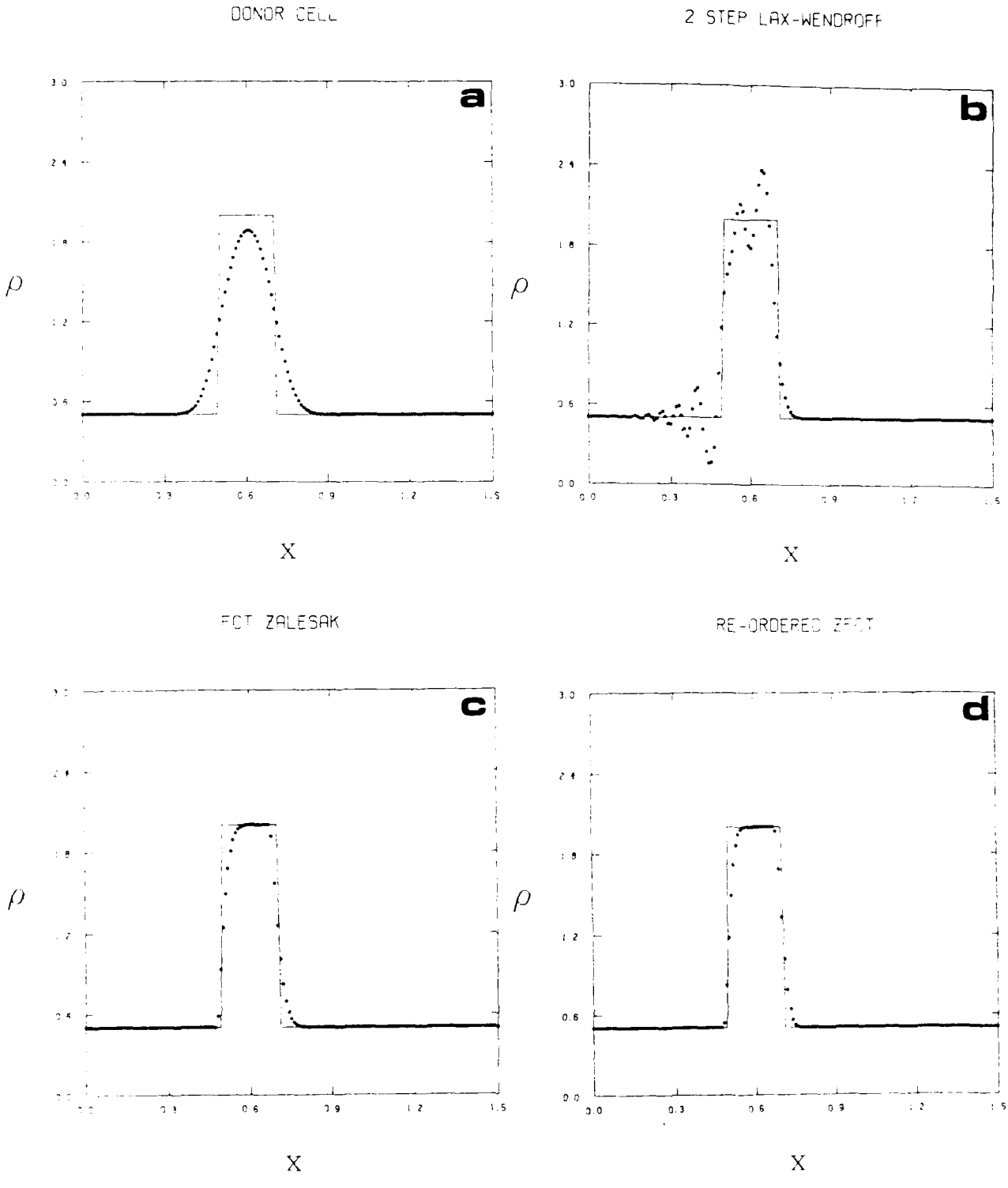

Figure 1. *The square-wave test at time* $t = 2.0$ *with* $\Delta t = \Delta x = 0.01$. *A square wave, which was initially 20 points wide, was advected at a constant velocity* $u = 0.2$. *The solid line represents the analytic solution and the dots are the computed solution, using* **a**) *the donor cell method,* **b**) *the two step Lax-Wendroff method,* **c**) *flux-corrected transport (ZFCT) as formulated by Zalesak (1979), and* **d**) *re-ordered Zalesak FCT (RZFCT) as formulated by Dietachmayer (1987).*

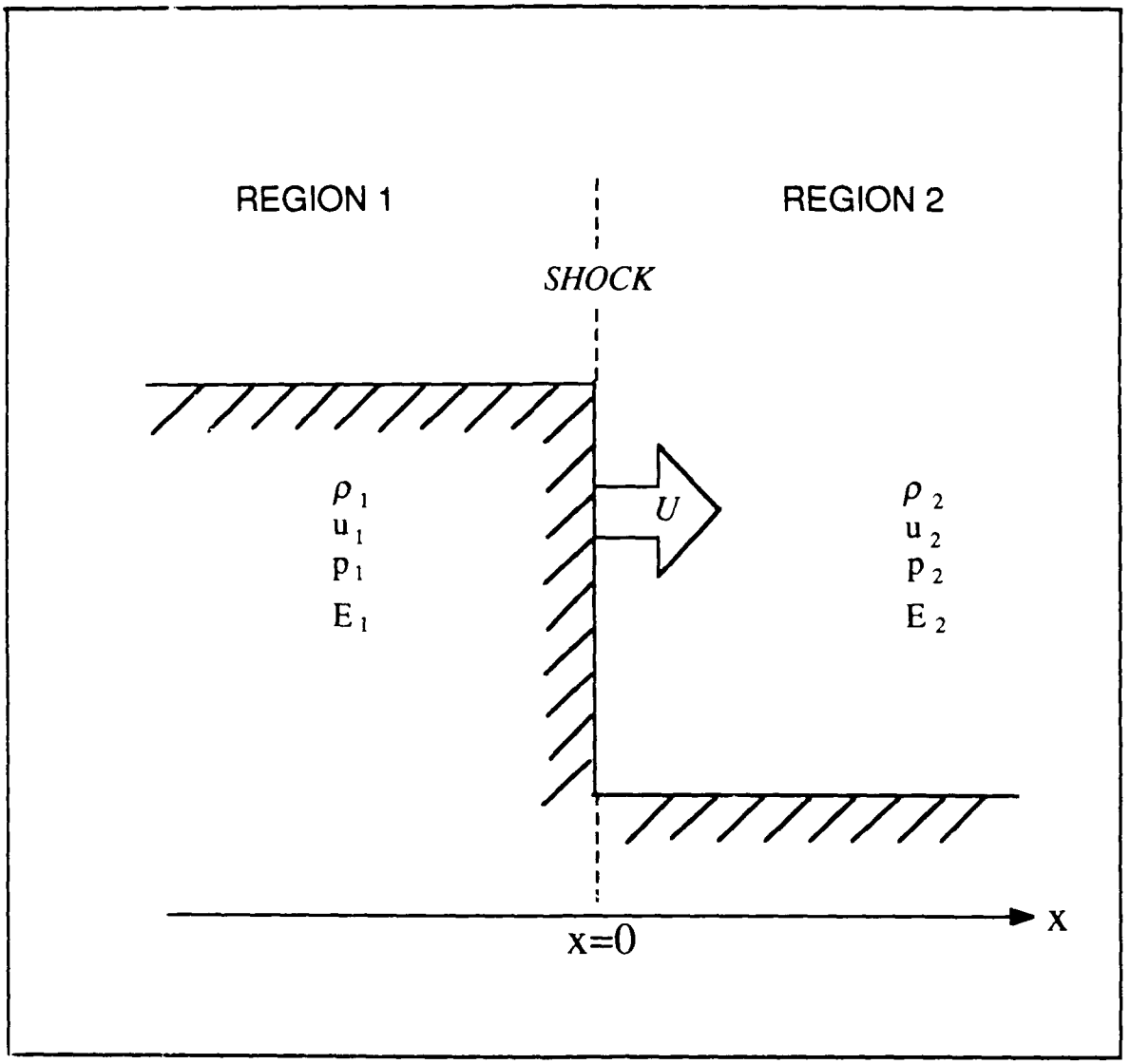

Figure 2. *Schematic diagram of the steady shock problem. A one-dimensional shock travels at velocity U through a uniform gas or metal.*

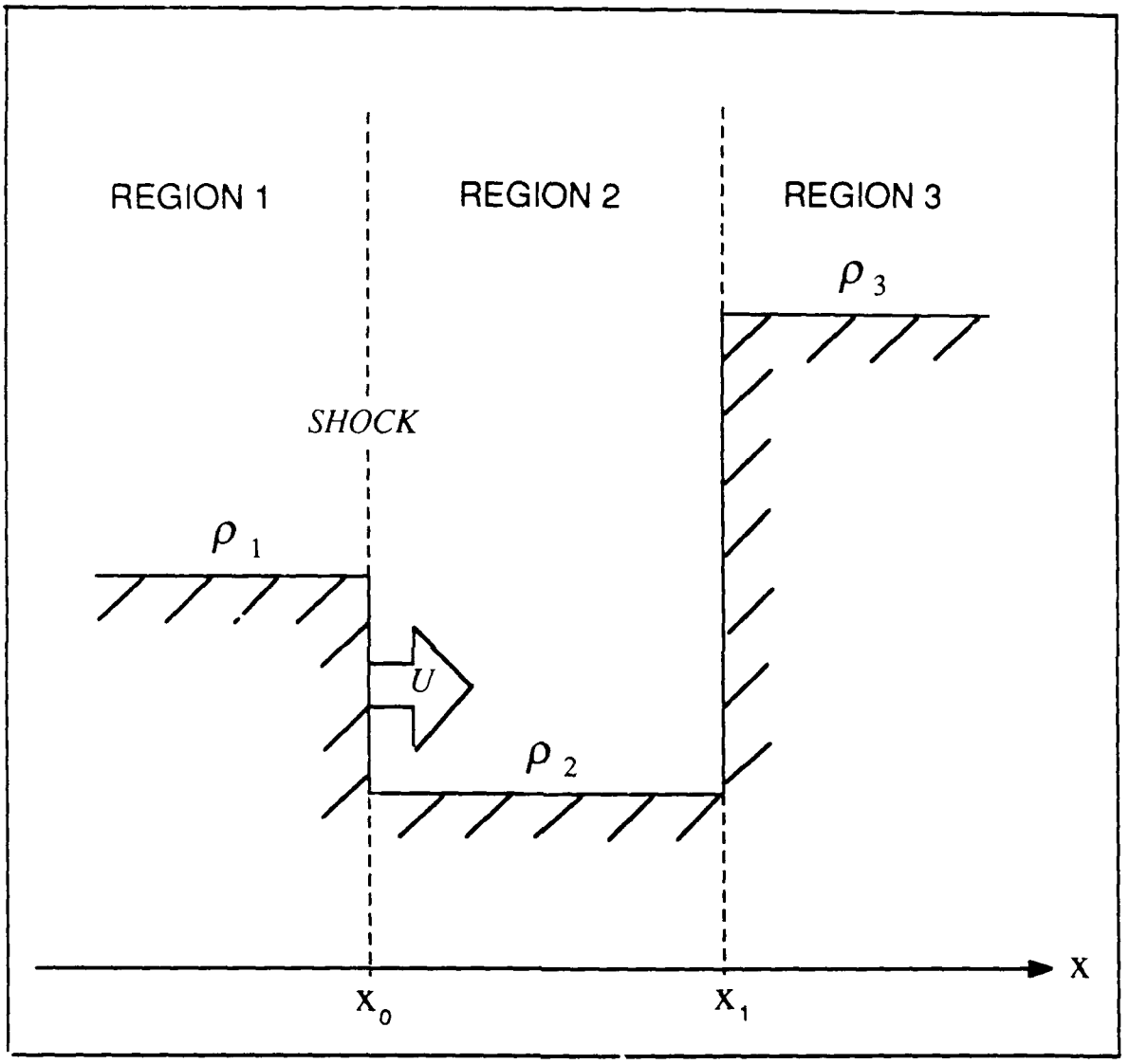

Figure 3. *Density distribution (at time $t = 0$) for a shock (initially at $x = x_o$) to hit a density discontinuity positioned at $x = x_1$. The density discontinuity is stationary.*

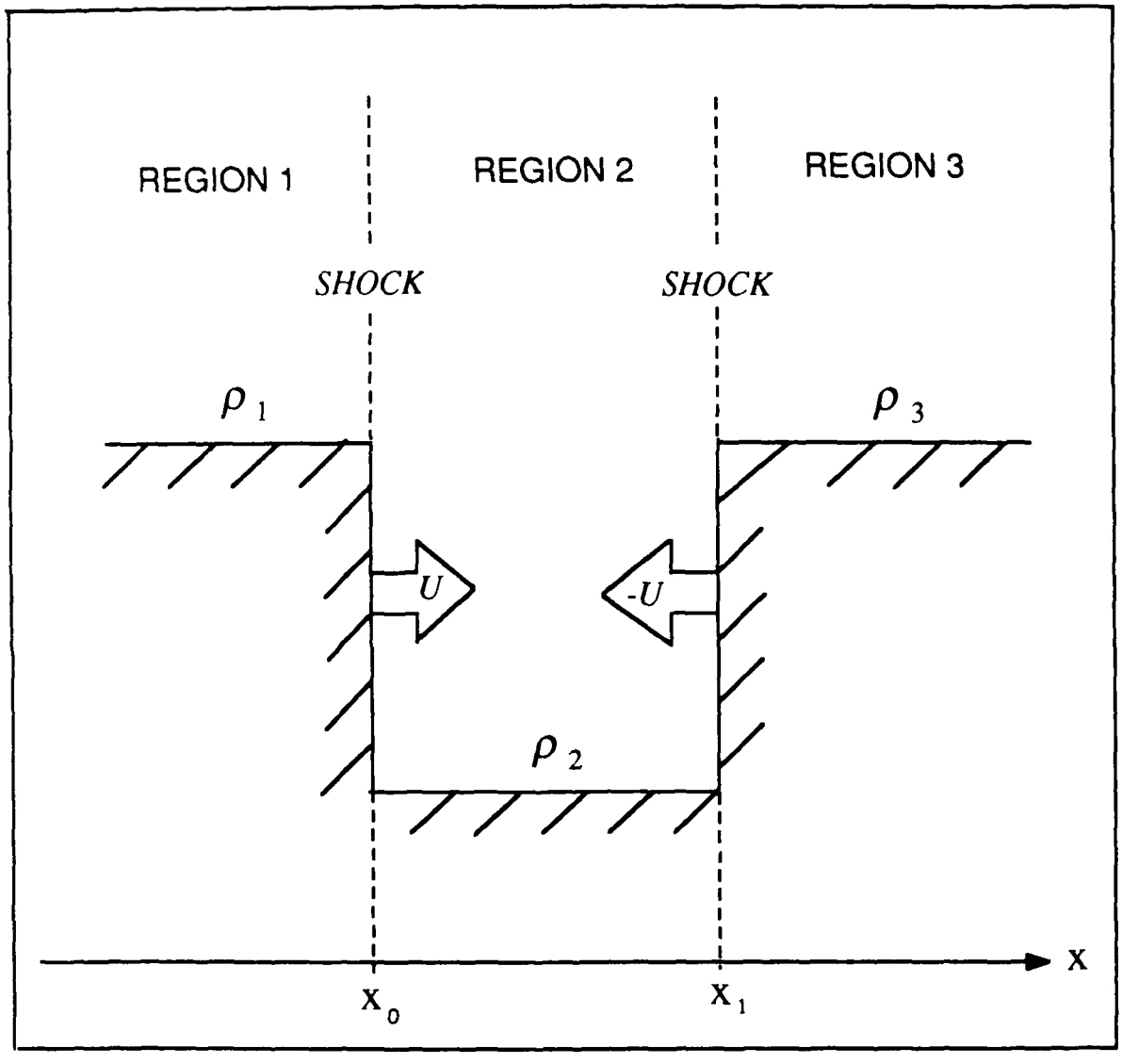

Figure 4. *Initial density distibution for two shocks (of equal stength), one at $x = x_o$ and the other at $x = x_1$, travelling in the opposite directions with absolute velocity U.*

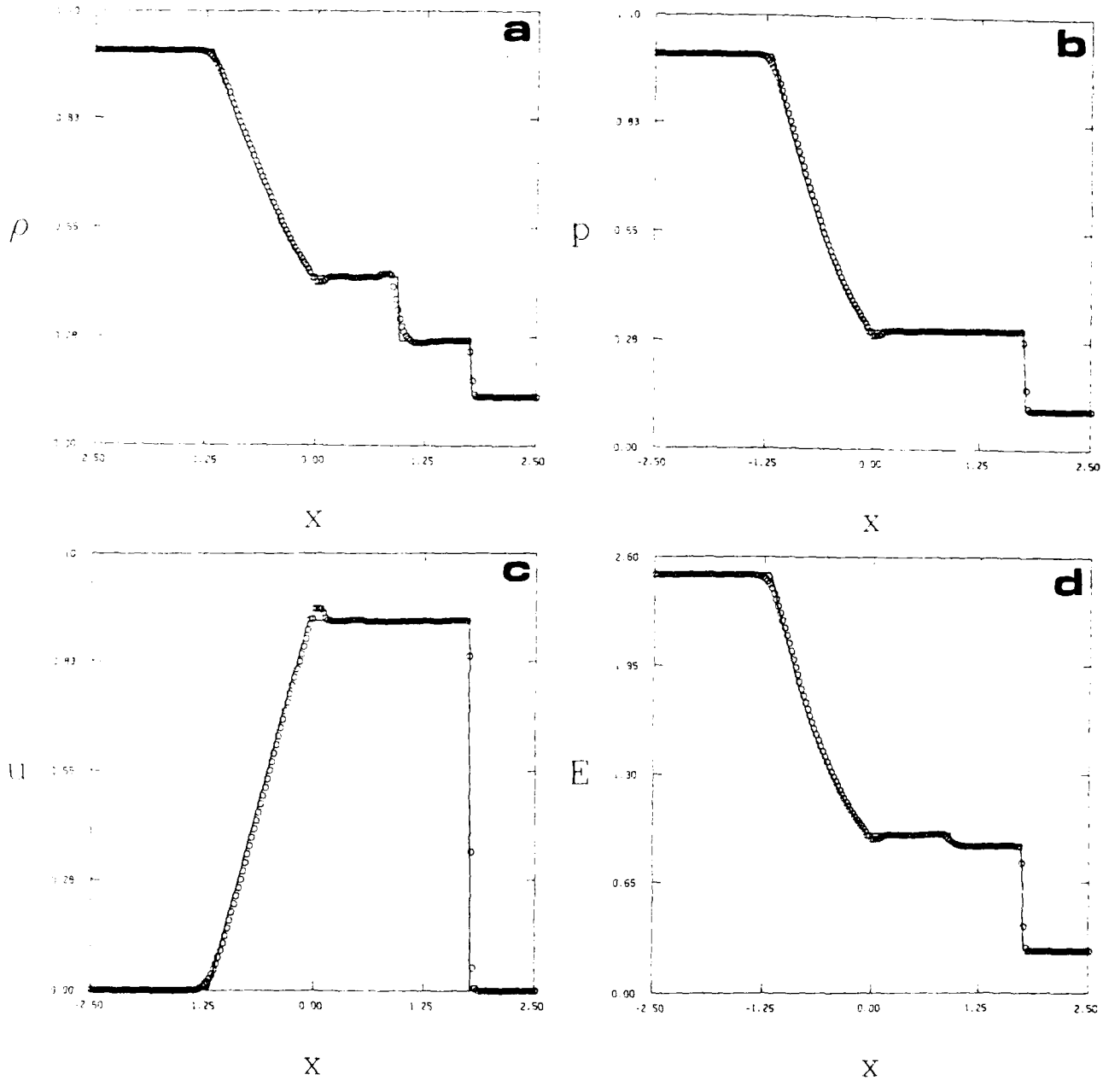

Figure 5. *The shock tube problem at time $t = 1.0$, with $\Delta x = 0.025$ and $\Delta t = 0.005$. The diaphragm was initially at $x = 0$. The circles represent the solution given by ZFCT and the solid line is the exact solution. The profiles for* **a)** *density,* **b)** *pressure,* **c)** *particle velocity, and* **d)** *total energy per unit volume are shown.*

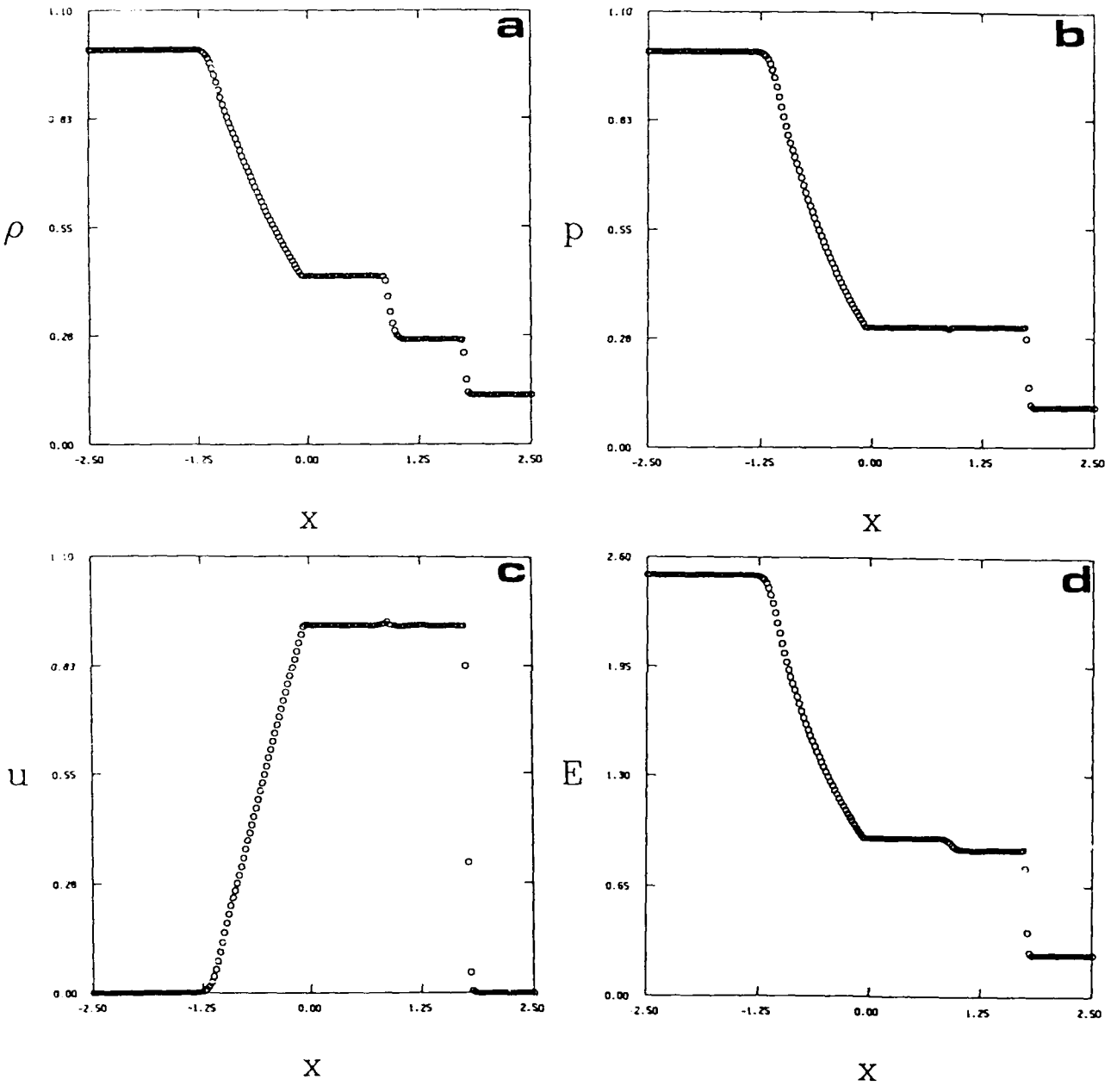

Figure 6. *The shock tube problem at time* $t = 1.0$, *with* $\Delta x = 0.025$ *and* $\Delta t = 0.005$. *The exact solution at time* $t = 0.5$ *was used as the initial conditions, then ZFCT was used to calculate the solution one hundred time steps later. The profiles for* **a**) *density,* **b**) *pressure,* **c**) *particle velocity, and* **d**) *total energy per unit volume are shown.*

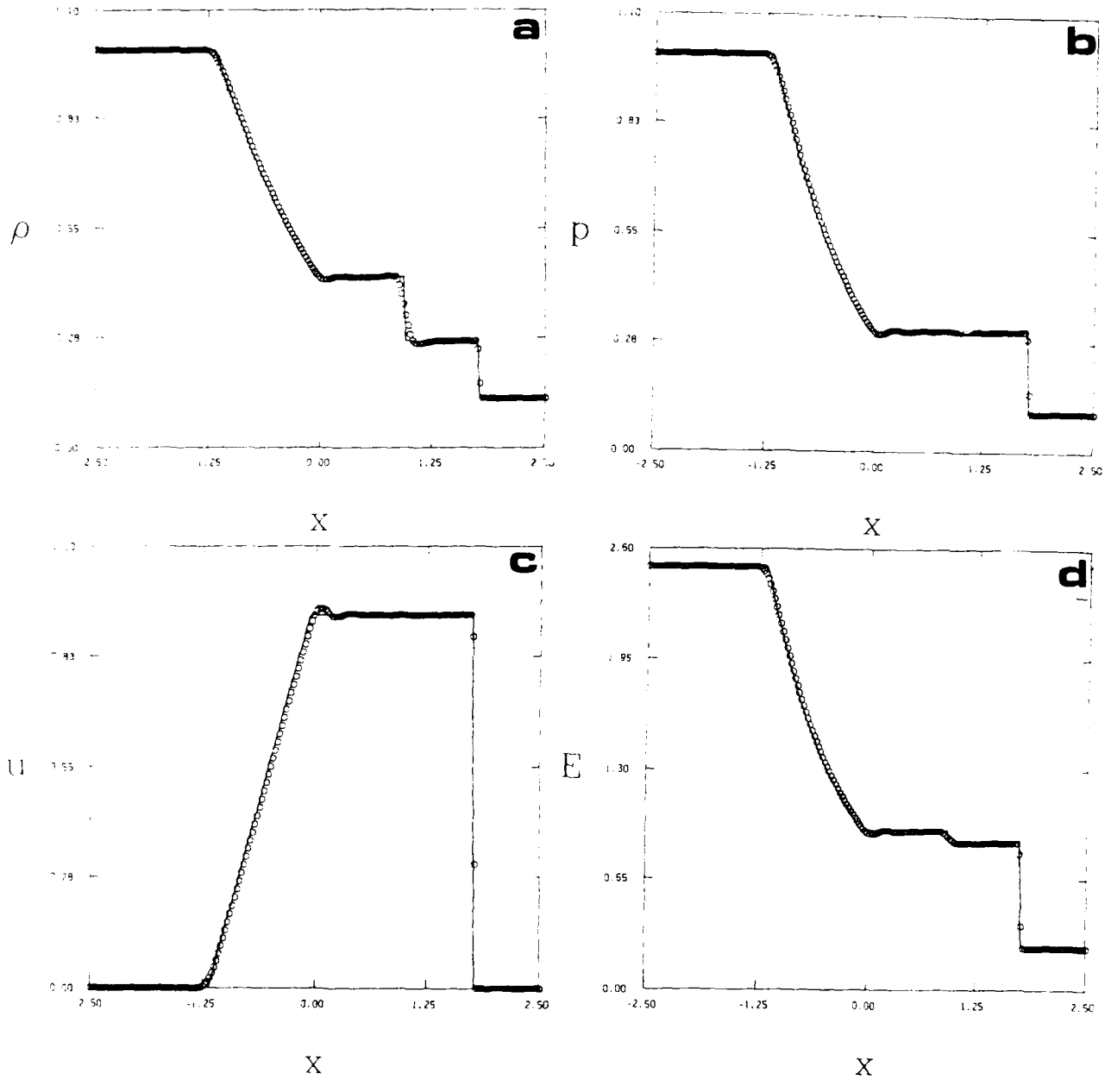

Figure 7. *Same as Fig. 5, except the circles represent the solution given by RZFCT.*

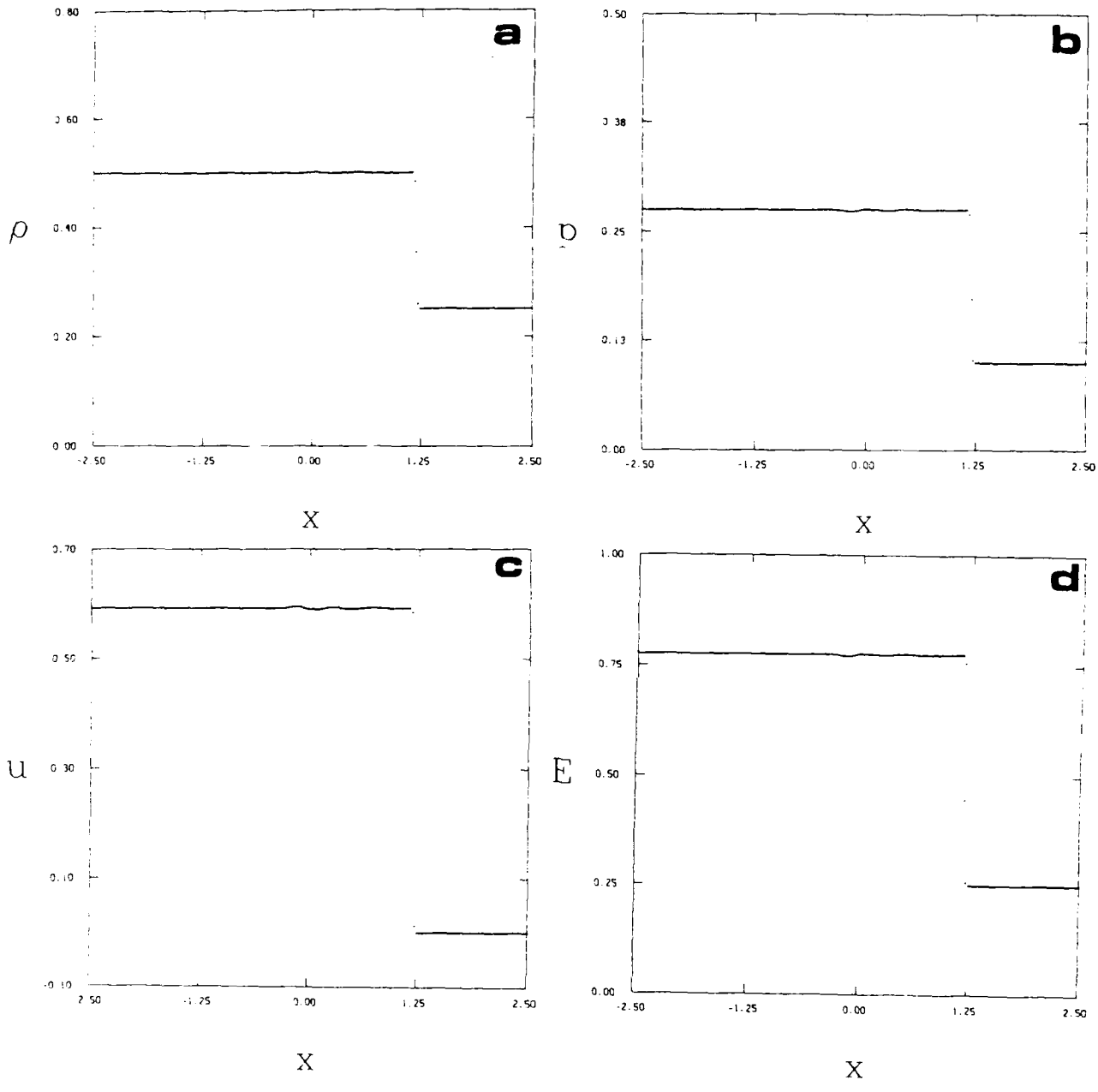

Figure 8. *The steady shock problem (in a gas) at time $t = 1.0$, with $\Delta t = 0.005$ and $\Delta x = 0.025$. The RZFCT profiles for* **a)** *density,* **b)** *pressure,* **c)** *particle velocity, and* **d)** *total energy per unit volume are shown. The shock was initially at $x = 0$.*

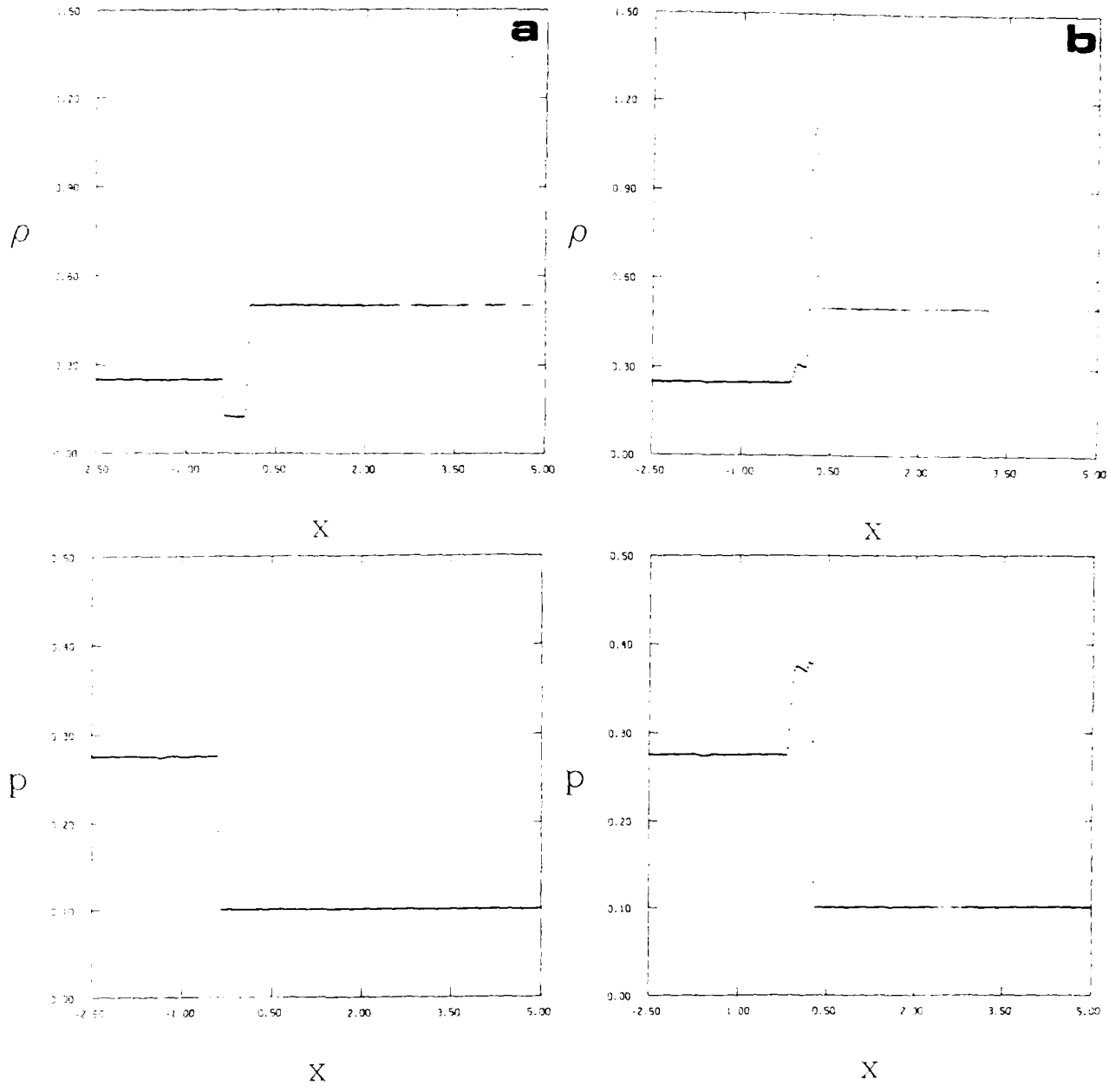

Figure 9. *The density and pressure profiles for a shock hitting a density discontinuity in a gas (using RZFCT), at time* **a)** $t = 0.5$ *and* **b)** $t = 1.0$. *The density discontinuity was positioned at* $x = 0$ *and the shock was initially at* $x = -1.25$.

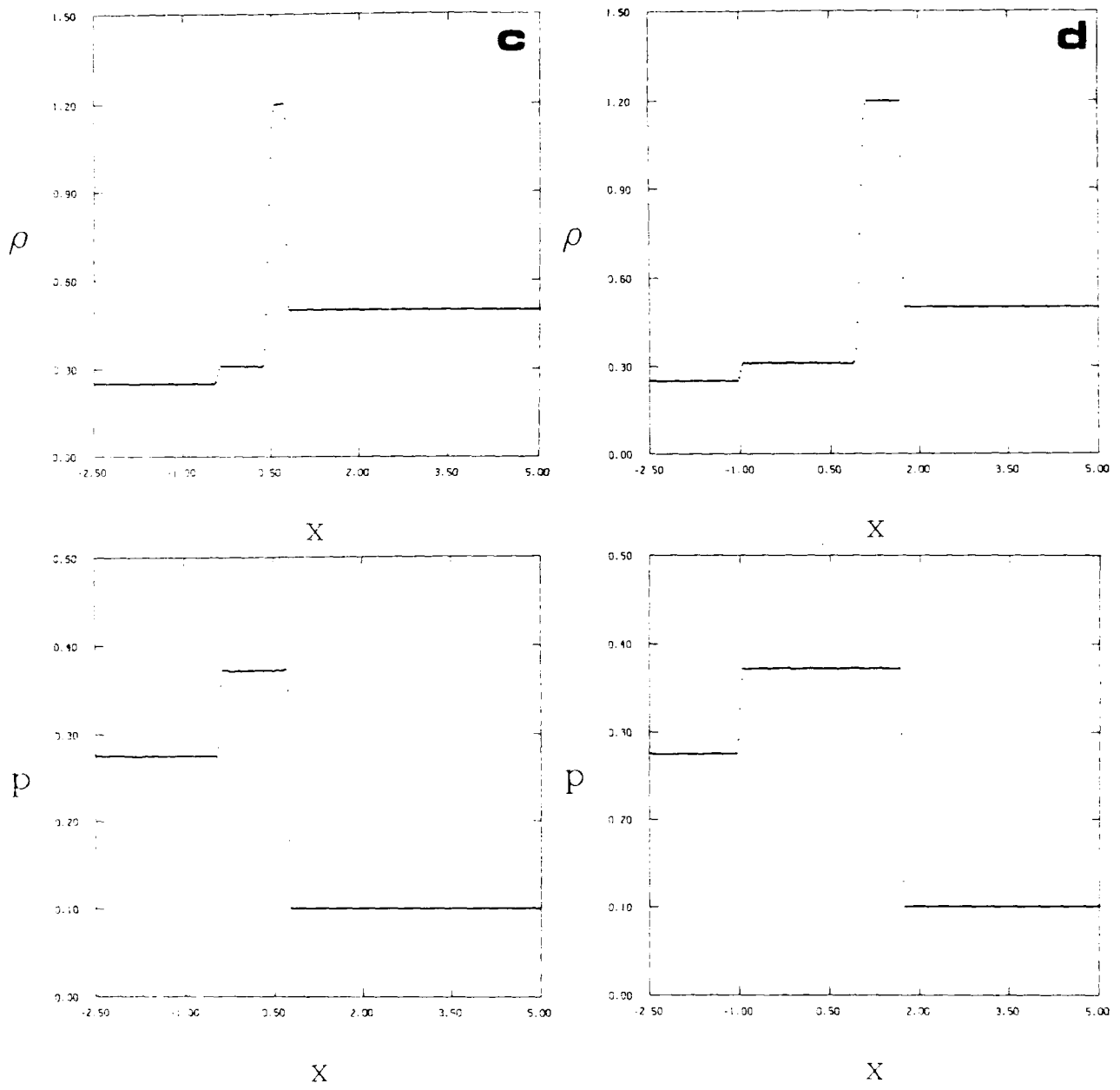

Figure 9, continued. *The density and pressure profiles at time* **c)** $t = 1.5$ *and* **d)** $t = 2.5$.

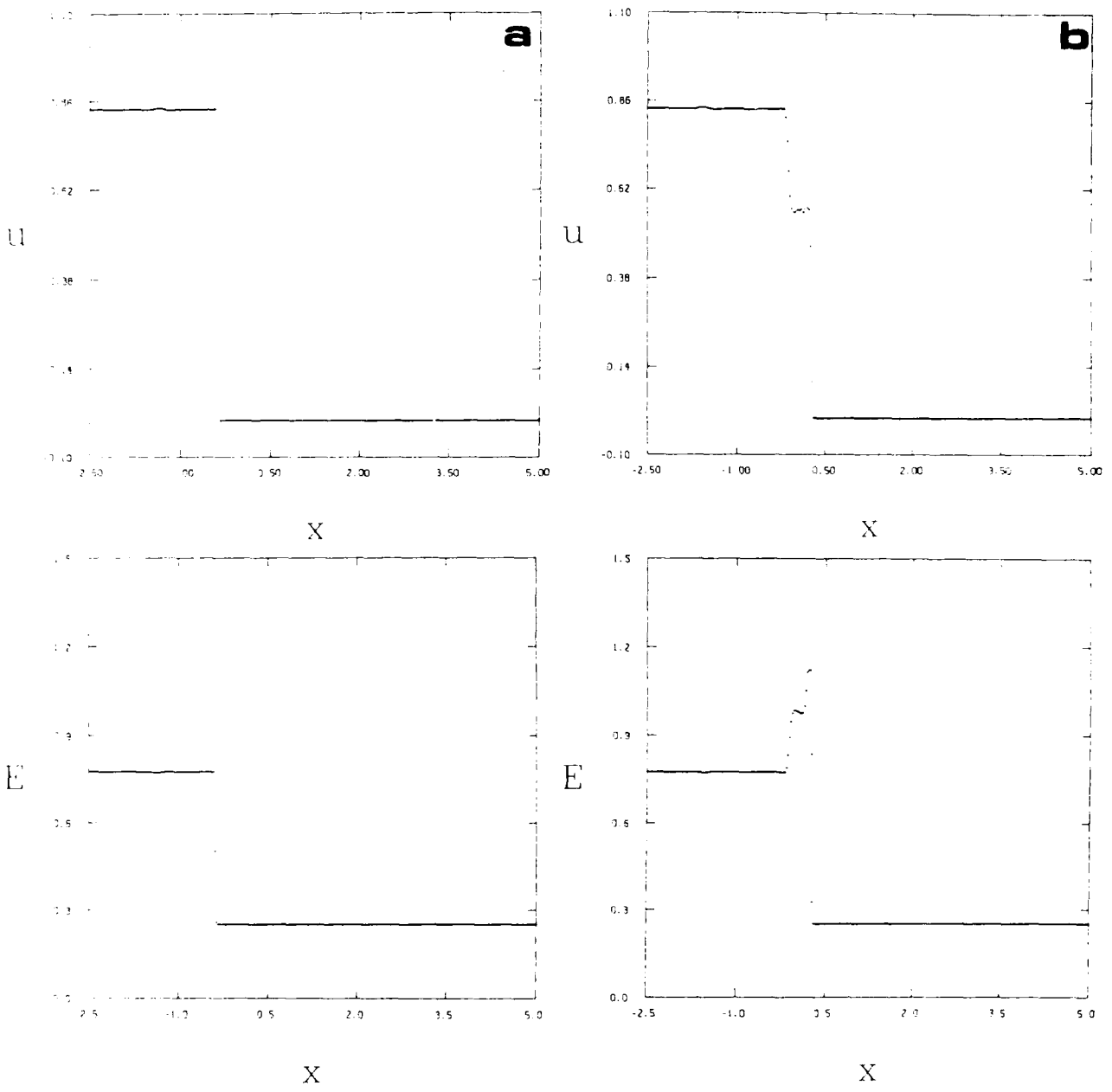

Figure 10. *Same as Fig. 9, except the particle velocity and total energy per unit volume profiles at time* **a)** $t = 0.5$ *and* **b)** $t = 1.0$.

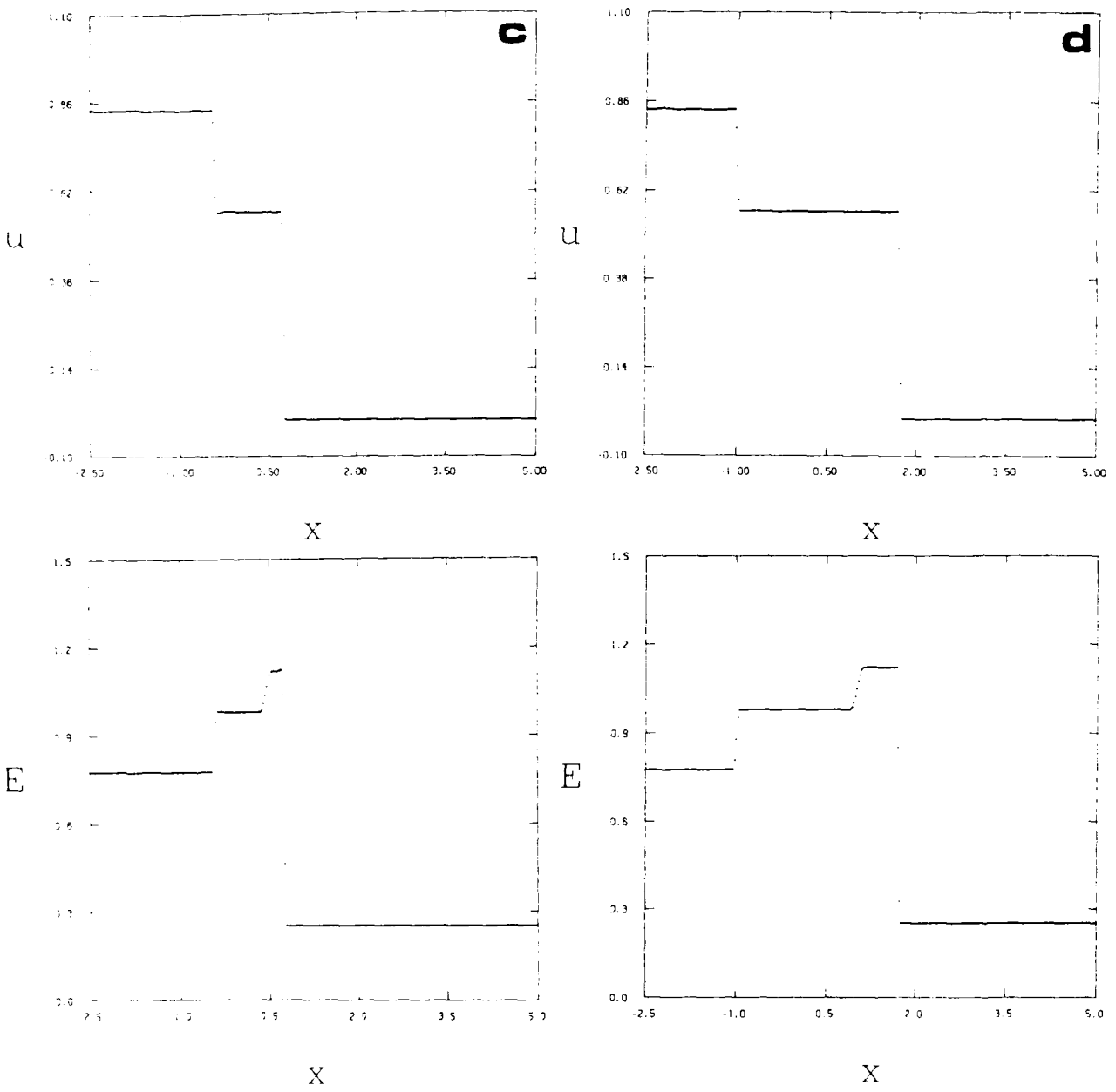

Figure 10, continued. *The particle velocity and total energy per unit volume at time* **c)** $t = 1.5$ *and* **d)** $t = 2.5$.

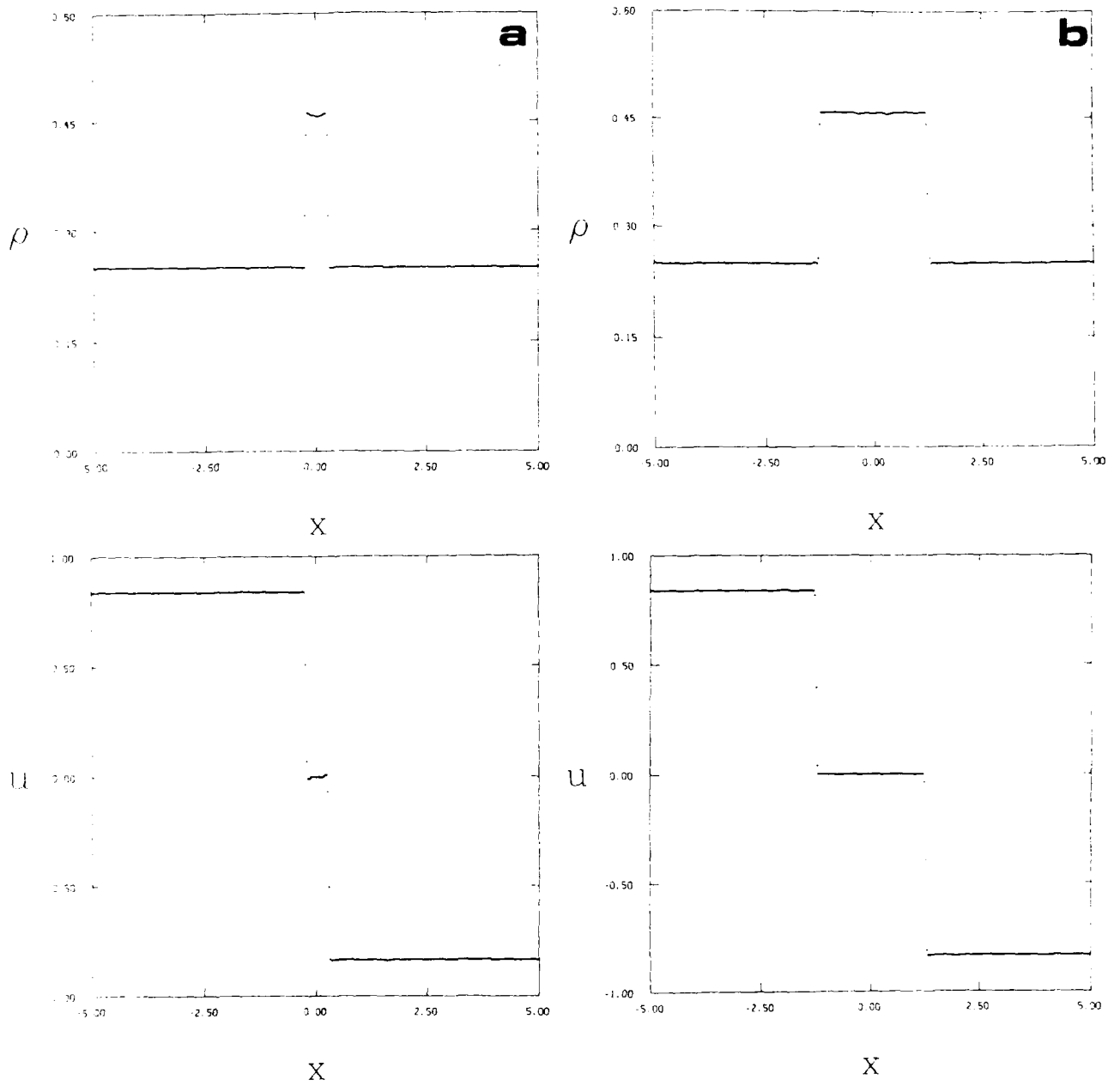

Figure 11. *The density and particle velocity profiles for the collision of two equal strength shocks in a gas (using RZFCT), at time* **a)** $t = 1.0$ *and* **b)** $t = 2.0$. *Initially the shocks were positioned at* $x = -1.25$ *and* $x = 1.25$, *with* $\Delta t = 0.005$ *and* $\Delta x = 0.025$.

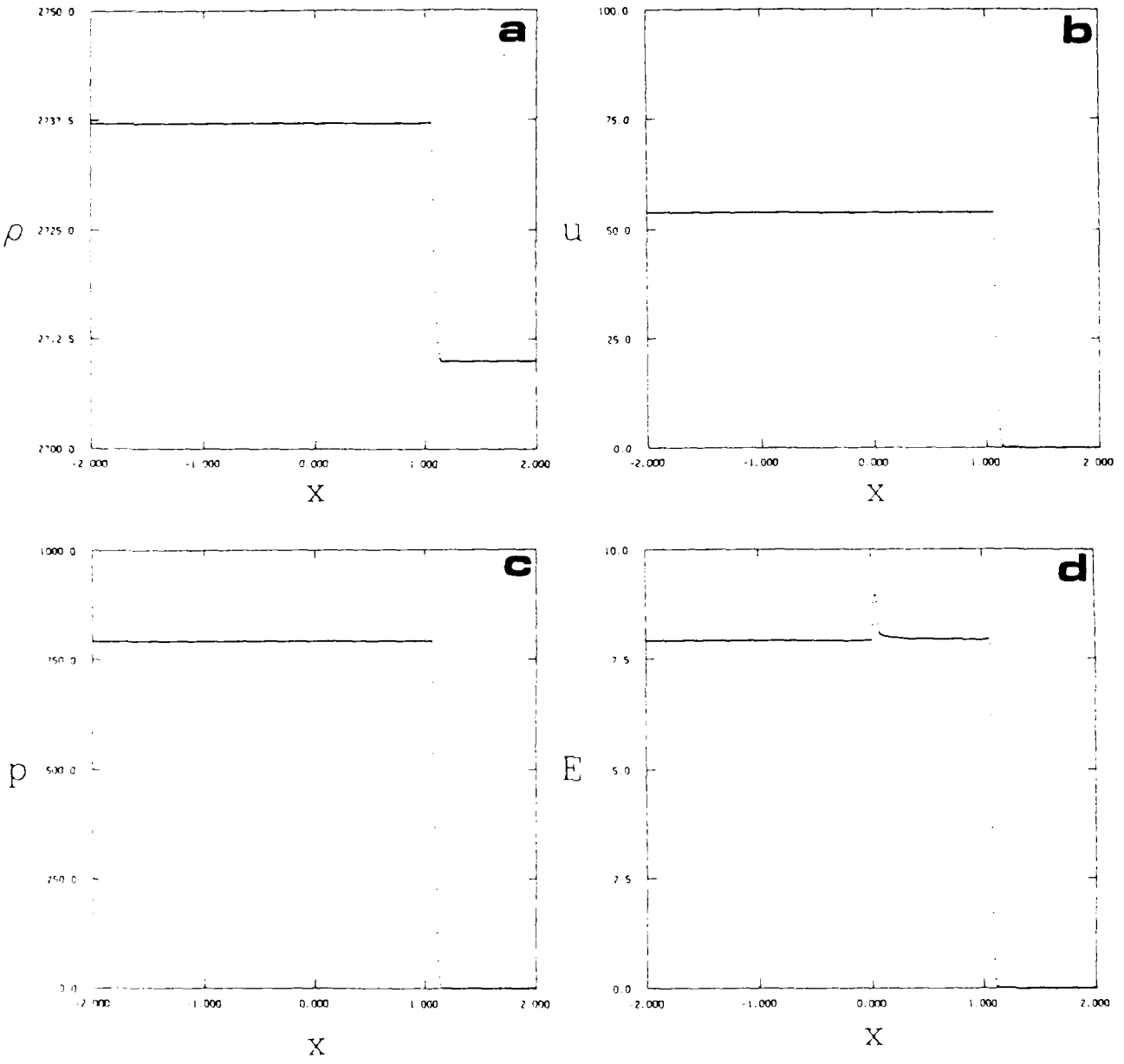

Figure 12. *The steady shock problem in aluminium at time* $t = 2.0 \times 10^{-4}\,s$, *with* $\Delta t = 5.0 \times 10^{-7}\,s$ *and* $\Delta x = 0.01\ m$. *The RZFCT profiles for* **a**) *density* ρ $(kg\,m^{-3})$, **b**) *particle velocity* u $(m\,s^{-1})$, **c**) *pressure* p *(MPa), and* **d**) *total energy per unit volume* E $(MJ\,m^{-3})$ *are shown. The shock was initially at* $x = 0.0\ m$. *The length scale* x *is in metres.*

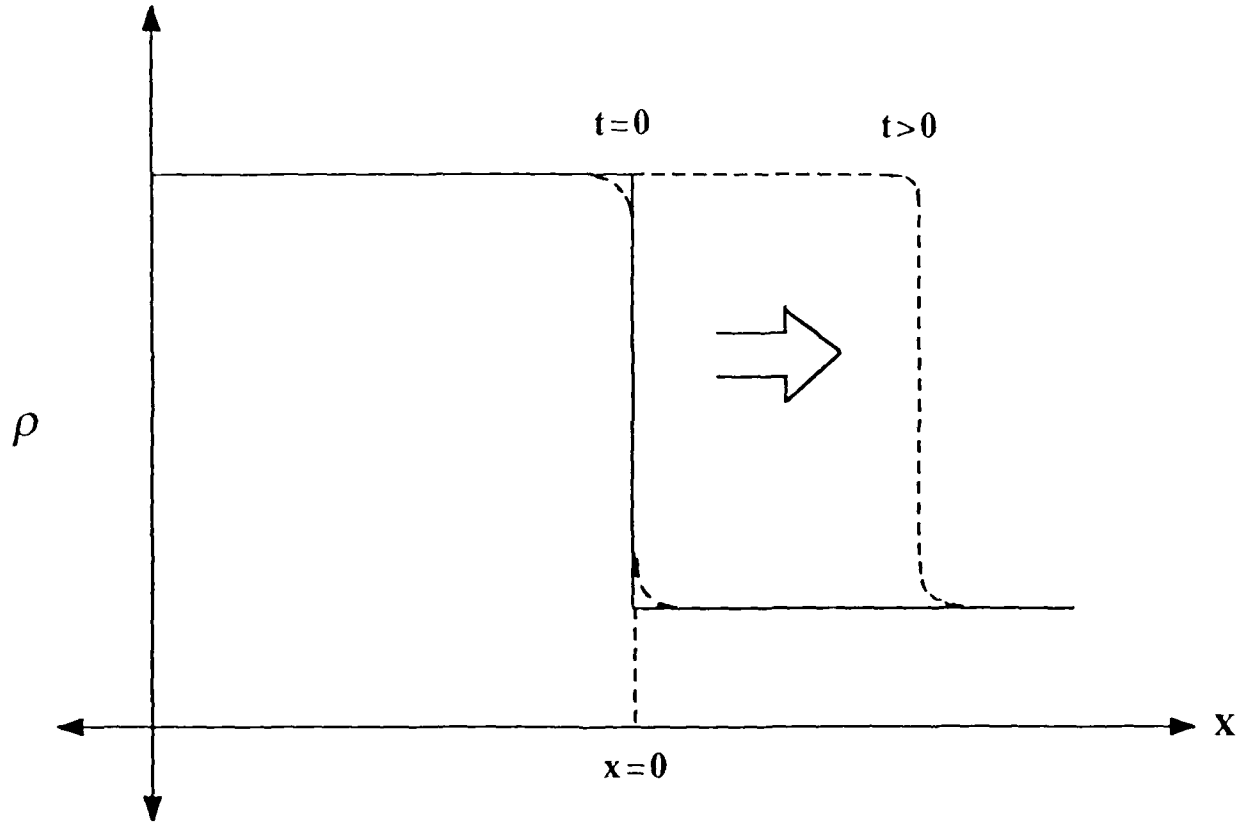

Figure 13. *Schematic diagram of the steady shock problem. The solid line represents the theoretical shock and the dashed line represents the numerical solution.*

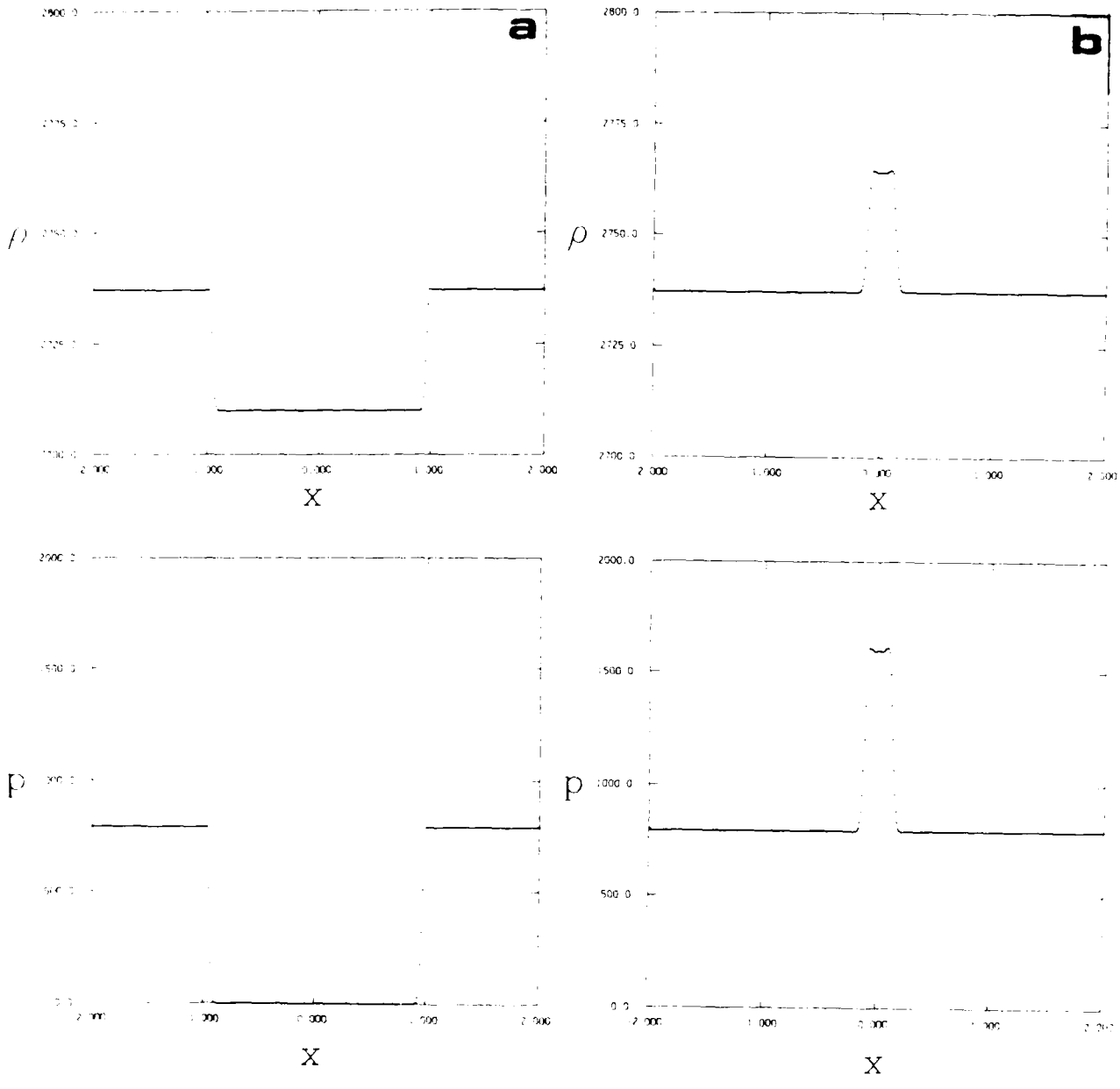

Figure 14. *The density ρ ($kg\,m^{-3}$) and pressure p (MPa) profiles for the collision of two equal strength shocks in aluminium at time* **a)** $t = 1.0 \times 10^{-4}\ s$ *and* **b)** $t = 3.0 \times 10^{-4}\ s$. *The RZFCT solution is shown where* $\Delta t = 5.0 \times 10^{-7}\ s$ *and* $\Delta x = 0.01\ m$. *The shocks were initially at* $x = -1.5\ m$ *and* $x = 1.5\ m$.

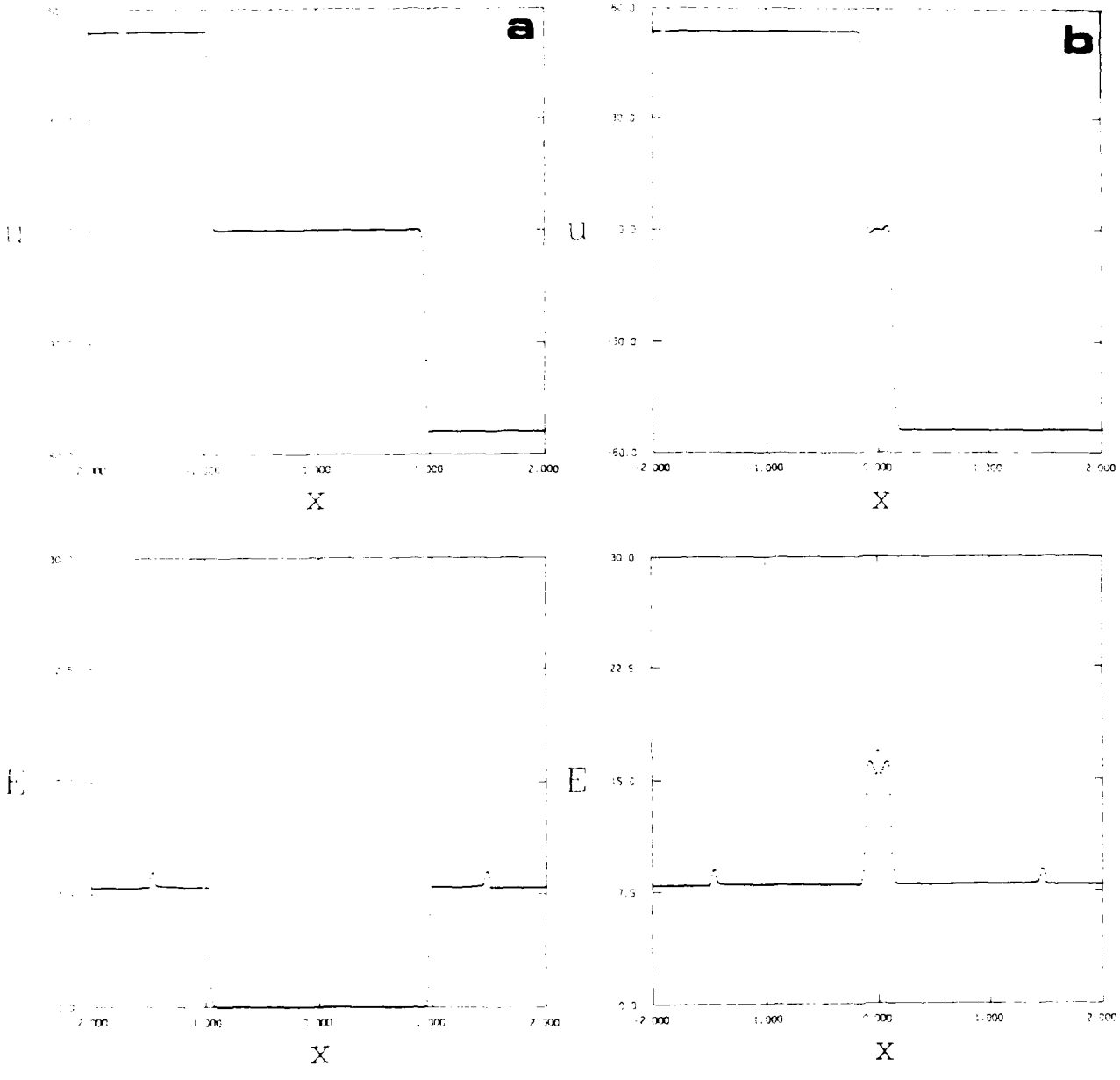

Figure 15. *Same as Fig. 14, except the particle velocity u ($m\,s^{-1}$) and total energy per unit volume E ($MJ\,m^{-3}$) at time* **a)** $t = 1.0 \times 10^{-4}\ s$ *and* **b)** $t = 3.0 \times 10^{-4}\ s$.

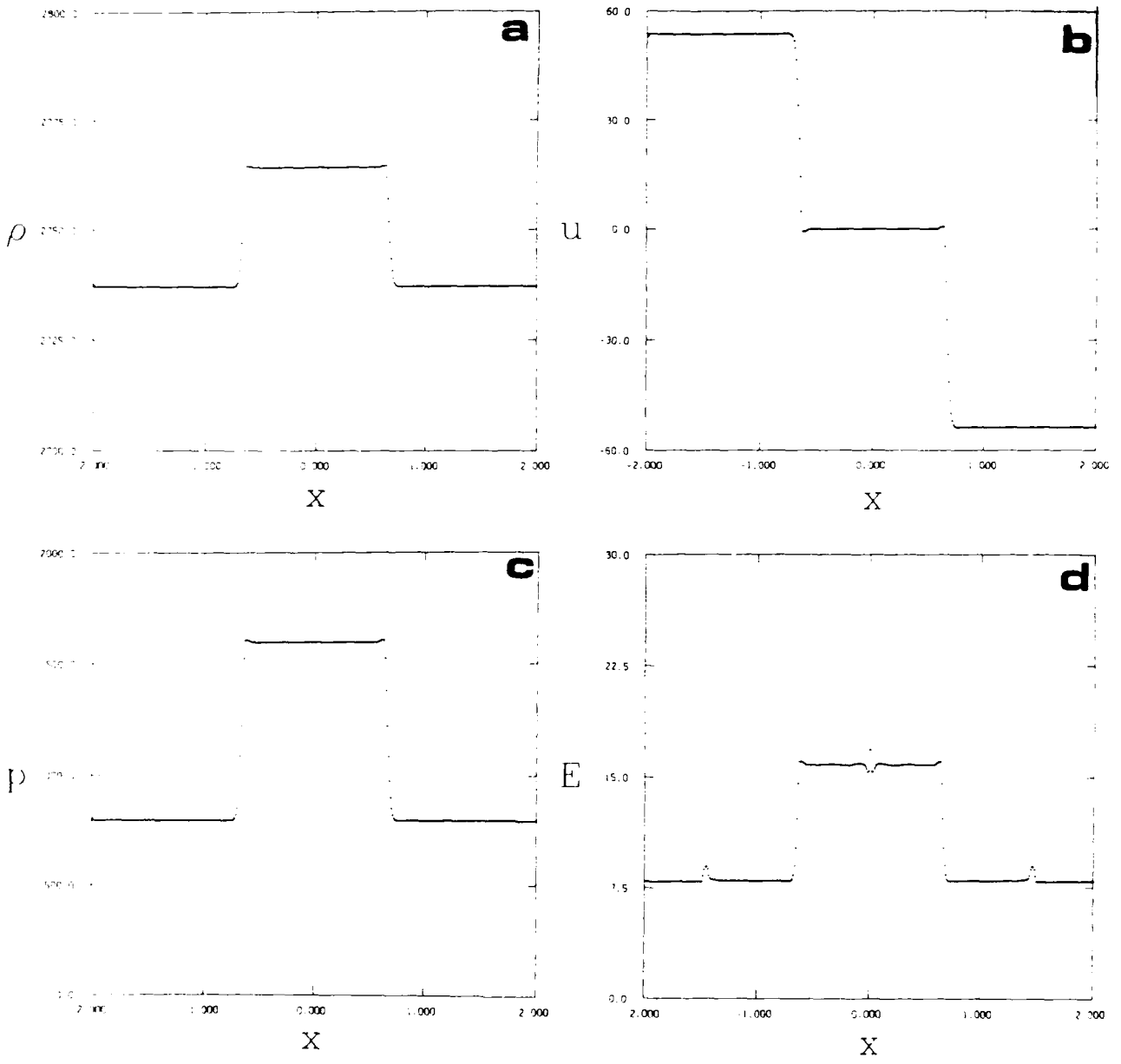

Figure 16. *Same as Fig. 14, except the* **a)** *density* ρ $(kg\,m^{-3})$, **b)** *particle velocity* u $(m\,s^{-1})$, **c)** *pressure* p *(MPa), and* **d)** *total energy per unit volume* E $(MJ\,m^{-3})$ *at time* $t = 4.0 \times 10^{-4}\,s$.

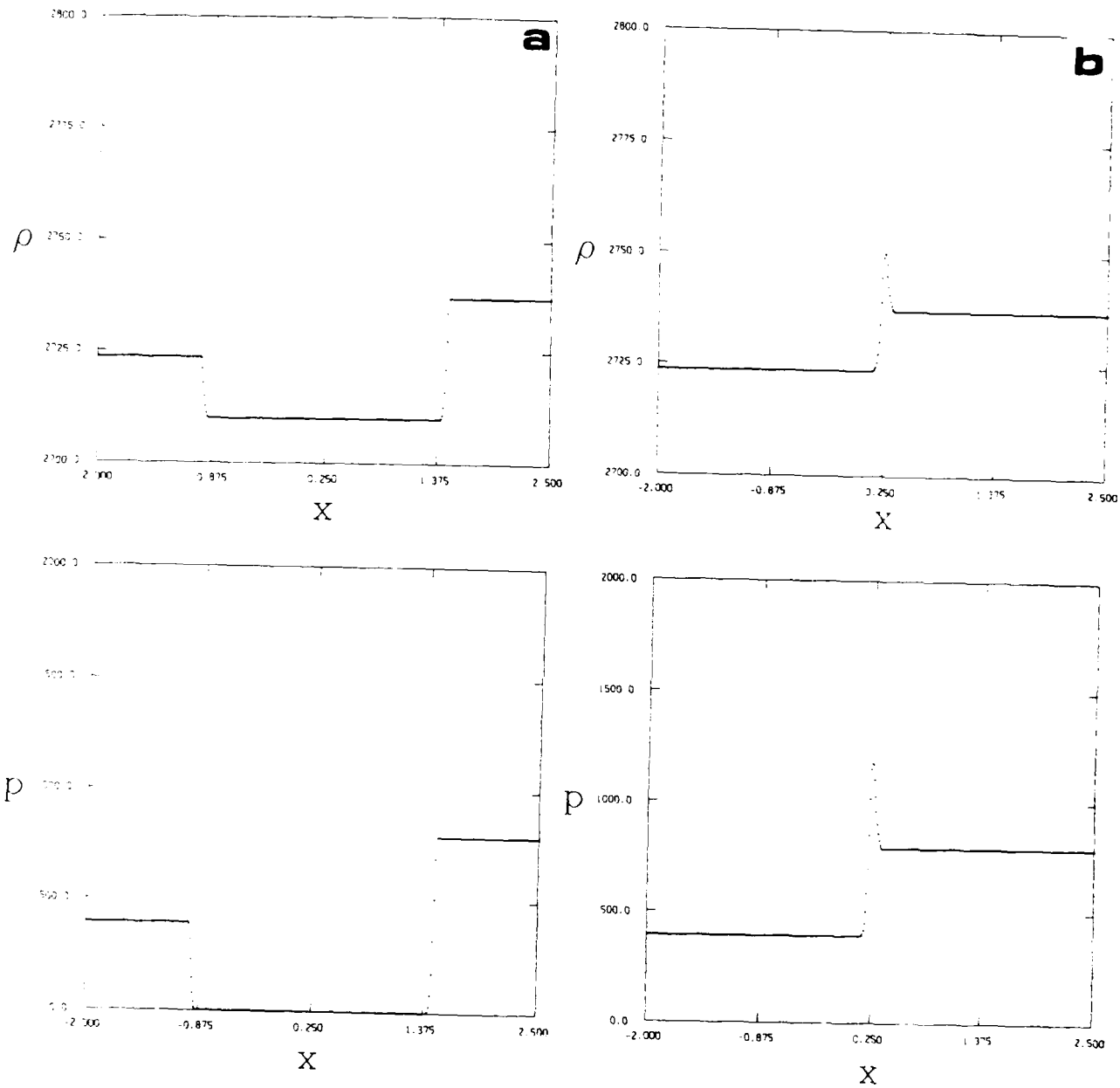

Figure 17. *The density ρ ($kg\,m^{-3}$) and pressure p (MPa) profiles for the collision of two shocks (of different strengths, see Table 3) in aluminium at time* **a)** $t = 1.0 \times 10^{-4}\ s$ *and* **b)** $t = 3.3 \times 10^{-4}\ s$. *The RZFCT solution is shown where* $\Delta t = 5.0 \times 10^{-7}\ s$ *and* $\Delta x = 0.01\ m$. *The shocks were initially at* $x = -1.5\ m$ *and* $x = 2.0\ m$.

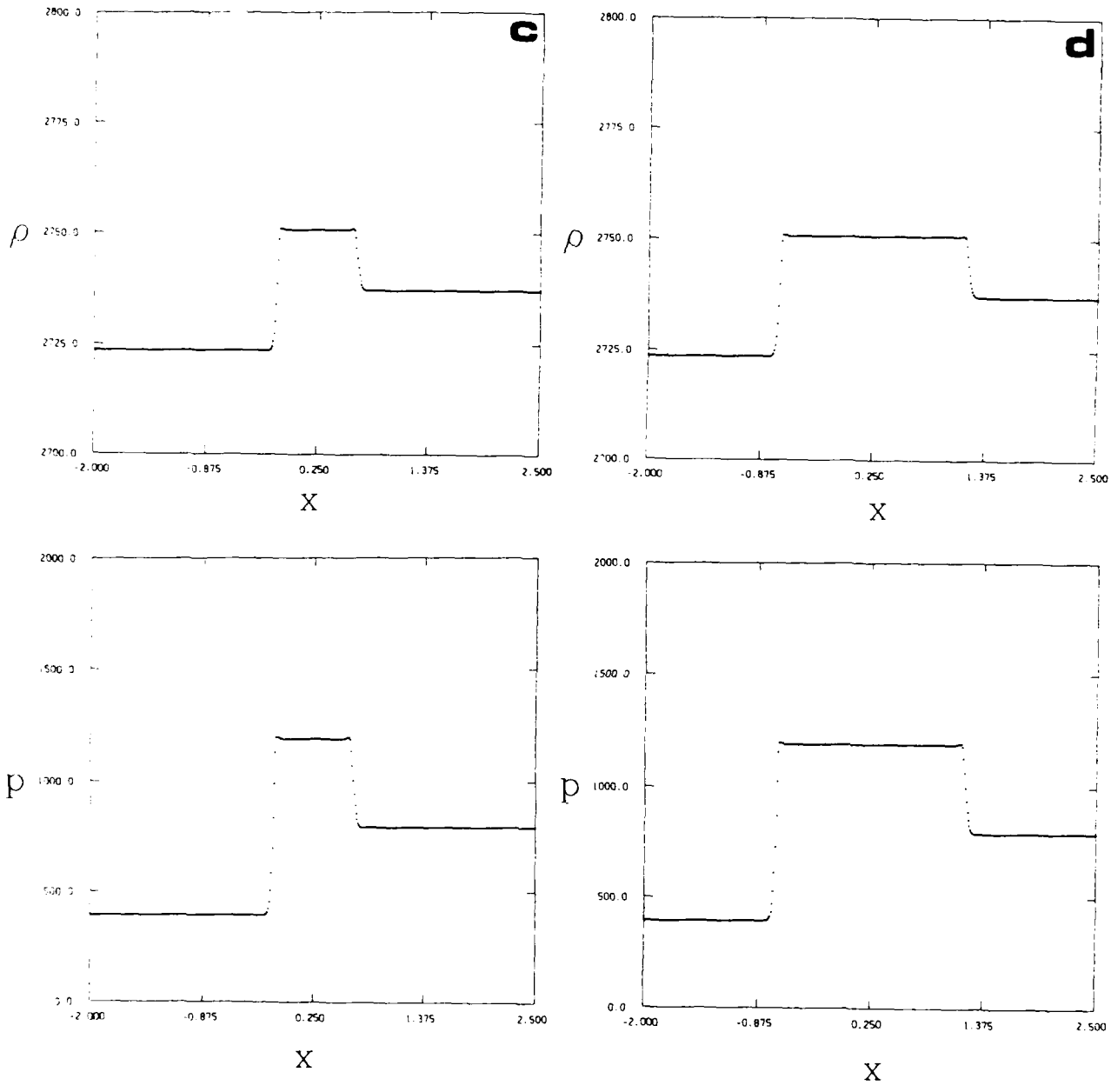

Figure 17, continued. *The density ρ ($kg\,m^{-3}$) and pressure p (MPa) profiles at time* **c)** $t = 4.0 \times 10^{-4}\ s$ *and* **d)** $t = 5.0 \times 10^{-4}\ s$.

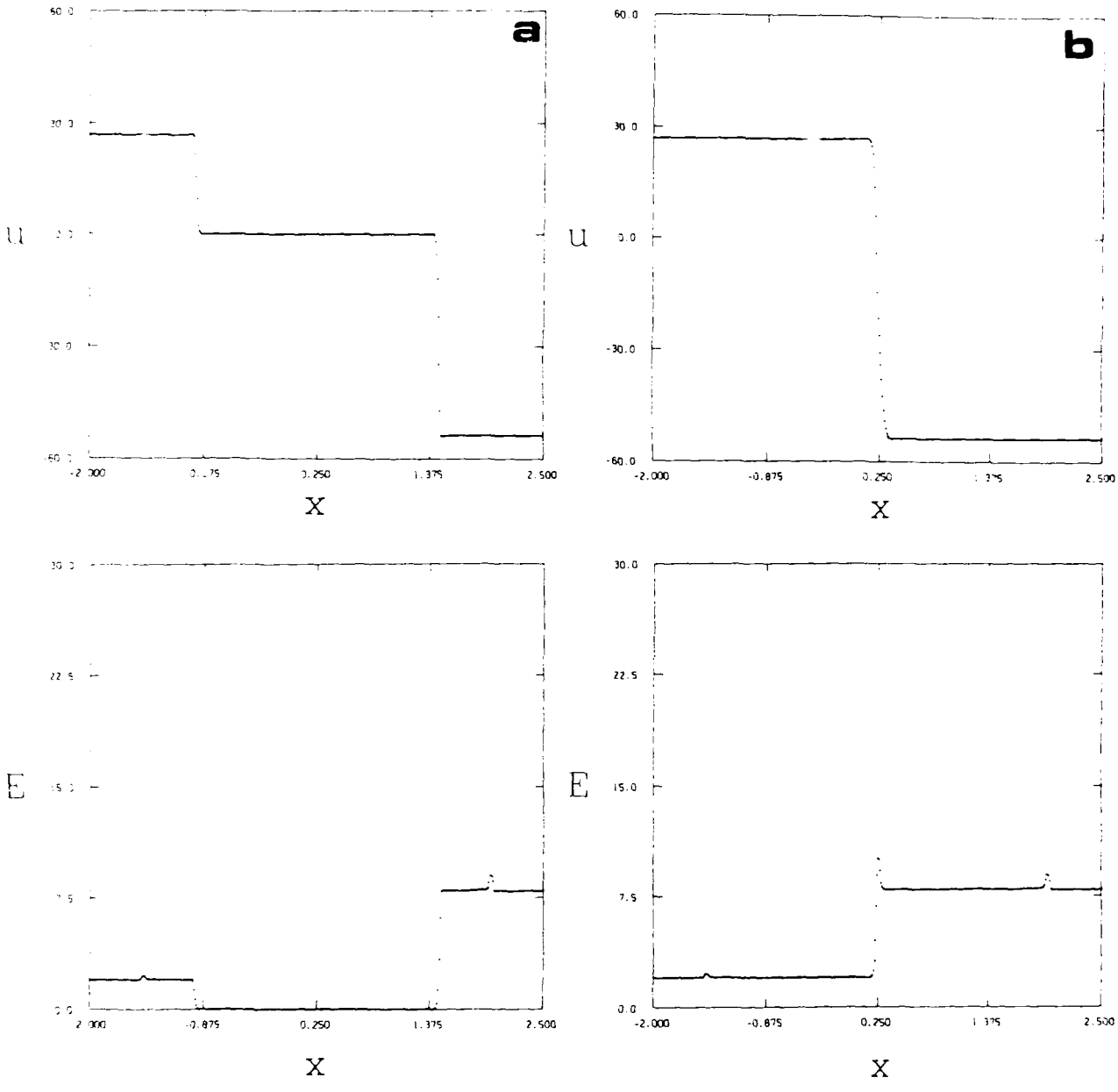

Figure 18. *Same as Fig. 17, except the particle velocity* u $(m\,s^{-1})$ *and total energy per unit volume* E $(MJ\,m^{-3})$ *at time* **a)** $t = 1.0 \times 10^{-4}\ s$ *and* **b)** $t = 3.3 \times 10^{-4}\ s$.

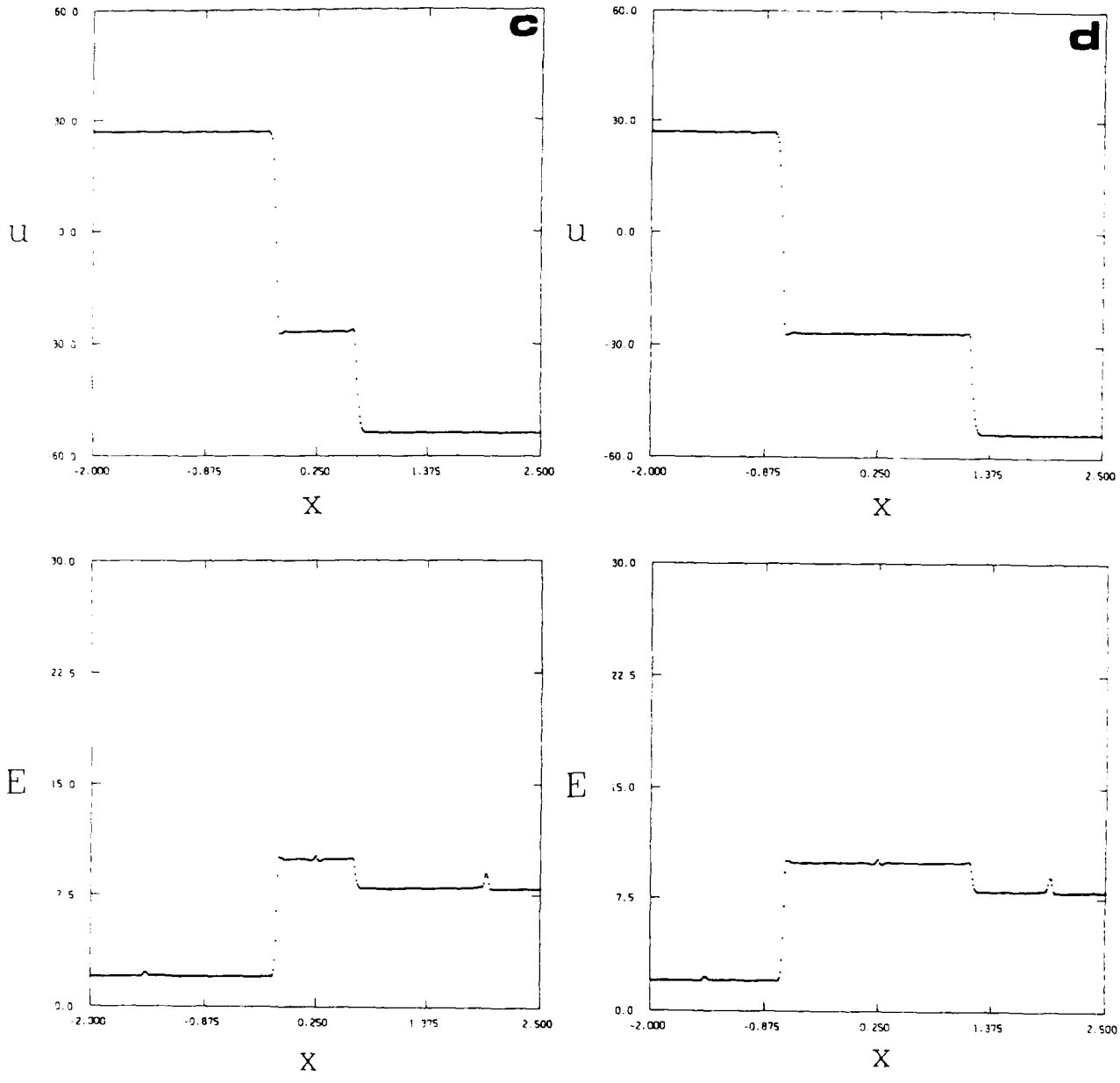

Figure 18, continued, *except the particle velocity* u $(m\,s^{-1})$ *and total energy per unit volume* E $(MJ\,m^{-3})$ *at time* **c)** $t = 4.0 \times 10^{-4}\,s$ *and* **d)** $t = 5.0 \times 10^{-4}\,s$.

SECURITY CLASSIFICATION OF THIS PAGE UNCLASSIFIED

DOCUMENT CONTROL DATA SHEET

REPORT NO.	AR NO.	REPORT SECURITY CLASSIFICATION
MRL-RR-8-89	AR-005-742	UNCLASSIFIED

TITLE
Numerical modelling of shocks in gases and metals

AUTHOR
M. B. Tyndall

CORPORATE AUTHOR
Materials Research Laboratory, DSTO
PO Box 50
Ascot Vale, Victoria 3032

REPORT DATE	TASK NO.	SPONSOR
September, 1989	DST 88/112	DSTO

FILE NO.	REFERENCES	PAGES
G6/4/8-3768	12	46

CLASSIFICATION/LIMITATION REVIEW DATE

CLASSIFICATION/RELEASE AUTHORITY
Chief, Explosives Division, MRL

SECONDARY DISTRIBUTION
Approved for Public Release

ANNOUNCEMENT
Announcement of this report is unlimited

KEYWORDS

Shock Waves	Modelling	Shock Fronts
Shock Loads	Shock Mechanics	Blast Effects

SUBJECT GROUPS
0072B 0079E

ABSTRACT
Results are presented for a range of one-dimensional shock wave problems in gaseous and metallic materials. These problems were solved numerically using Flux-Corrected Transport (FCT). FCT is a numerical technique which achieves high resolution without non-physical oscillations, especially in regions of steep gradients such as shock fronts.

These types of problem involve solving the Eulerian inviscid fluid flow equations, namely the continuity equation, conservation of momentum and conservation of energy, with an appropriate equation of state. For gaseous materials the ideal gas equation of state was used and for metallic materials the "stiffened-gas" or the Mie-Grüneisen equation of state. Shock wave problems in gases included the one-dimensional shock tube problem, a shock wave hitting a density discontinuity and shocks of equal magnitude

ABSTRACT (CONTINUED)
colliding. Using the "stiffened-gas" equation of state and the Mie-Grüneisen equation of state similar types of problems were solved for metallic materials, for example, a shock propagating through a piece of metal.

A discussion of the performance of FCT to accurately model these problems is given. Currently work is being done on adding elastic-plastic (or viscous) terms and heat conduction terms to the fluid flow equations, to improve the description of flow in a solid material.